Thermal Investigation of the Green Revolution Energy Converter

– A study on the heat transfer within the GREC in regards of temperature distribution and heat rate.

Emma Andersson, emman355
Emma Gustafsson, emmgu210
Maja Abrahamsson Bolstad, majbo091
Matilda Eriksson, mater368
Wilma Fager, wilfa164

LINKÖPINGS UNIVERSITET

Linköping University
Division of Management and Engineering
Project Report | 2023-01-11

Abstract

To reduce emissions, new technological solutions can be of use. One technology which is currently being developed is the Green Revolution Energy Converter, GREC. GREC is an engine with the aim to produce electricity from temperature gradients.

This project is part of a greater project that is divided in two with different focus areas. These two projects aim to deliver a specification of the next step of the prototype, called: Lab Model v3, which is expected to be built in spring 2023. The aim of this report is to contribute with new knowledge about the heat transfer on the hot section of the GREC model. The goal is to design the heat block and conductive fin, HB and CF, to deliver high amount of heat to a volume of air which is called the work generating volume, WGV. This includes evaluating two different heat transfer techniques which in this report are called None Pipe Heat Transfer, NPHT, and Pipe Heat Transfer, PHT. The temperature distribution within the CF and the HB, as well as the heat transfer to the WGV are analyzed.

This analysis is performed for different radii and thicknesses of the CF and HB, different flow rates of the heat carrier in the PHT case, and for different heat source temperatures to see if the two models are applicable in real life applications. The real life application for the NPHT model is a fuel cell vehicle and for the PHT model a district heating system.

To obtain the result, ANSYS Workbench is used to create the model of GREC and MATLAB is used to calculate heat transfer coefficient and pressure losses. Furthermore, an iterative method using COMSOL Multiphysics and ANSYS Workbench was necessary to obtain temperatures of the CF, HB and WGV. The chosen method for this study comes with several uncertainties. However the trends seen in the results can still be considered credible, but exact numbers and other detailed conclusions should be avoided.

For the NPHT model, a large model in terms of radius and thickness, results in the highest total heat rate. This is due to the combination of a large CF and heat source area. The NPHT model with smallest radius and largest thickness results in the most even temperature distribution for the NPHT cases.

The PHT model presents a more even temperature distribution on the surface of the CF than the NPHT model. The largest heat rate from the different configurations derived from the PHT model is approximately three times larger than the heat rate derived from the NPHT model with the same dimensions. Moreover, a higher flow rate on the water in the pipes of the PHT model, does not affect the heat rate or temperature distribution on the CF. Therefore, a lower flow rate could be applied to save pump power. Another conclusion to this project is that the PHT model could be applicable in a district heating system with 80 °C, since the heat transfer coefficient values do not differ much between 80 °C and 100 °C. The NPHT model might also be applicable in a real life application. In that case, the size of CF plays a larger role than the temperature of the heat source in terms of the possible heat rate output. A final conclusion is that size, type of heat source and design of the GREC plays a vital role in terms of temperature distribution on CF and heat rate to WGV. The GREC has the potential to be applicable in real life applications in regards of heat transfer solutions.

Acknowledgement

We would like to thank our project owner Nils Karlberg, for inspiration and encouragement, our counsellor Johan Renner, for technical and academical advices, the previous project group (from spring 2022) for explanations and figures, and the other current project group IHT for assistance, fun meetings and computational help.

Table of Contents

Nomenclature

Symbol	Parameter	Unit
T_h	Temperature of the hot conductive fin	°C
T_c	Temperature of the cold conductive fin	°C
r_p	Pressure ratio	-
r_v	Volume ratio	-
$\dot{Q}$	heat rate	W
k	Thermal conductivity	$\frac{w}{mK}$
γ	Specific heat ratio	-
A	Area	m^2
b	Width	m
h	Heat transfer coefficient	$\frac{W}{m^2K}$
Nu	Nusselts number	-
L	Characteristic length	m
Re	Reynolds number	-
U	Fluid velocity	$\frac{m}{s}$
υ	Kinematic viscosity	$\frac{m^2}{s}$
Pr	Prandtls number	-
c_p	Specific heat capacity	$\frac{J}{KgK}$
μ	Dynamic viscosity	$\frac{Kg}{ms}$
d	Diameter	m
r	Radius	m
T_{WGV}	Temperature of WGV	°C
Δp	Pressure loss	Pa
ζ	Component dependent coefficient	-
ρ	Density	$\frac{kg}{m^3}$
λ	Friction factor	-
k_s	Roughness factor	-
P_{pump}	Pumping power	W
$\dot{v}$	Volume flow rate	$\frac{m^3}{s}$

Abbreviation	Explanation
GREC	Green Revolution Energy Converter
RS	Revolving Shutter
WGV	Work Generating Volume
TRL	Technology Readiness Level
PHT	Pipe Heat Transfer
NPHT	None Pipe Heat Transfer
HTC	Heat Transfer Coefficient
CF	Conductive Fin
HB	Heat Block
CB	Cold Block

1 Introduction

The severe impacts of green house gas emissions on the global warming is today a fact. The emissions can be coupled to several different sectors where heat and electricity production were the sectors with the highest increase of CO_2 emissions in 2021 [1]. To reduce emissions, new technological solutions can be of use. One technology which is currently being developed is the Green Revolution Energy Converter, further on mentioned as GREC. GREC is an engine with the aim to produce electricity from temperature gradients, which potentially can be applied in sectors like electricity production and transport.

1.1 Background

In this section, a background to the project is presented.

Company Description

nilsinside AB is an innovative technology company. The company is in the start of developing their product the GREC, described as a powerful sustainable motor [2]. The GREC engine aims to be climate positive. nilsinside AB strives to present a highly scalable, powerful, adjustable, low cost and zero carbon emission motor concept to contribute to the Paris Agreement goal, to limit global warming to 1.5 °C. The GREC is presented to be applicable in a wide range of industries with the purpose to mainly replace today's polluting combustion engines. nilsinside AB believes that their motor will be an efficient energy converter able to change how companies internationally generate emission-free and clean energy [2].

Technology Behind the GREC

The GREC is a new heat engine technology with the potential to transform low temperature gradients into power. The concept is to use an electric motor to move a volume of air between a hot and a cold space to create a pressure difference. The construction of the GREC can be seen in Fig. 1. The GREC consists of one hot block, HB, and one cold block, CB, which respectively includes several conductive fins, CF. The revolving shutter, RS, is a pack of discs in the closed GREC with the purpose of moving around gas in the open area between the CFs. The RS is not in contact with the fins and is operated freely by an electric stepper motor [3]. The gaseous volume column that the RS is moving, is kept within a quarter of an opening and is called work generating volume, WGV. When the RS rotate, it repetitively moves the WGV between the CF of the HB and the CF of the CB. From this motion the temperature of the WGV repeatedly increase and decrease rapidly. This rapid change in temperature results in an internal pressure change. The faster rotation, the more energy can be converted. To prevent unwanted efficiency leaks between the hot and cold conductive areas, isolating "nil blocks" are placed in between these areas [3].

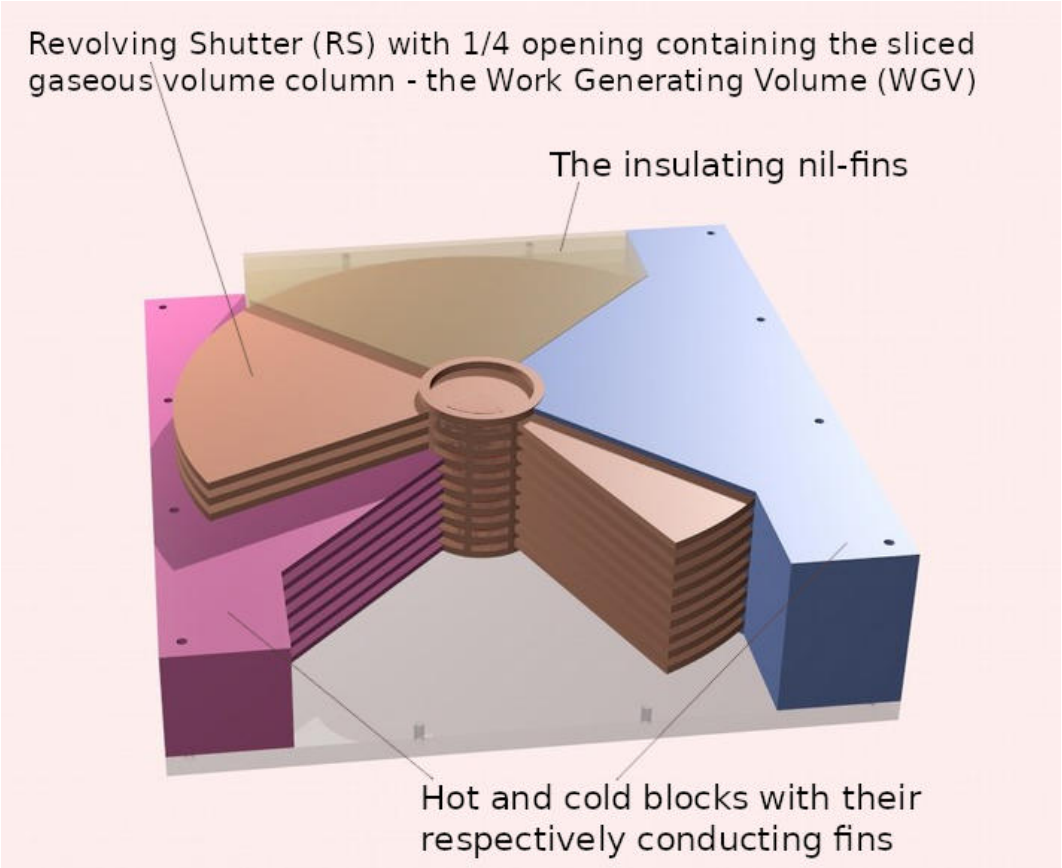

Figure 1: A representation of how the GREC is built with descriptive texts for different the parts. The HB and CB together with their connected CF, are in the figure shown as the pink and blue parts respectively. The electric operated RS is shown in brown. The insulating nil-fins are shown in transparent beige, where the nil-fins closest to the viewer has been removed to be able to showcase the inside of the GREC [3].

To give a better explanation of how the GREC engine work, Fig. 2 is presented. This figure illustrate four steps of how the WGV rotates for one revolution of the RS. Fig. 2 (a) illustrates the initial contact with WGV and the HB. In this step, heat is transferred to the WGV, resulting in a rise of temperature and pressure. WGV will be forced to expand and an external piston will be pushed creating mechanical work. After the expansion of the volume, the pressure will drop again but the temperature of the WGV will be relatively constant. When there is no heat transfer from the HB anymore, the WGV is located in the isolated area between the CB and HB, see (b) in Fig. 2. In Fig. 2 (c) the heat from WGV will be transferred to the CB and this leads to a drop in both temperature and pressure. The pressure drop will force the atmospheric pressure to push back the piston since the volume retracts. The pressure will start to rise again and the temperature will continue to be relatively constant. This occurs until the WGV is located in the isolated area between the HB and CB, Fig. 2 (d), which concludes one revolution of the RS [4].

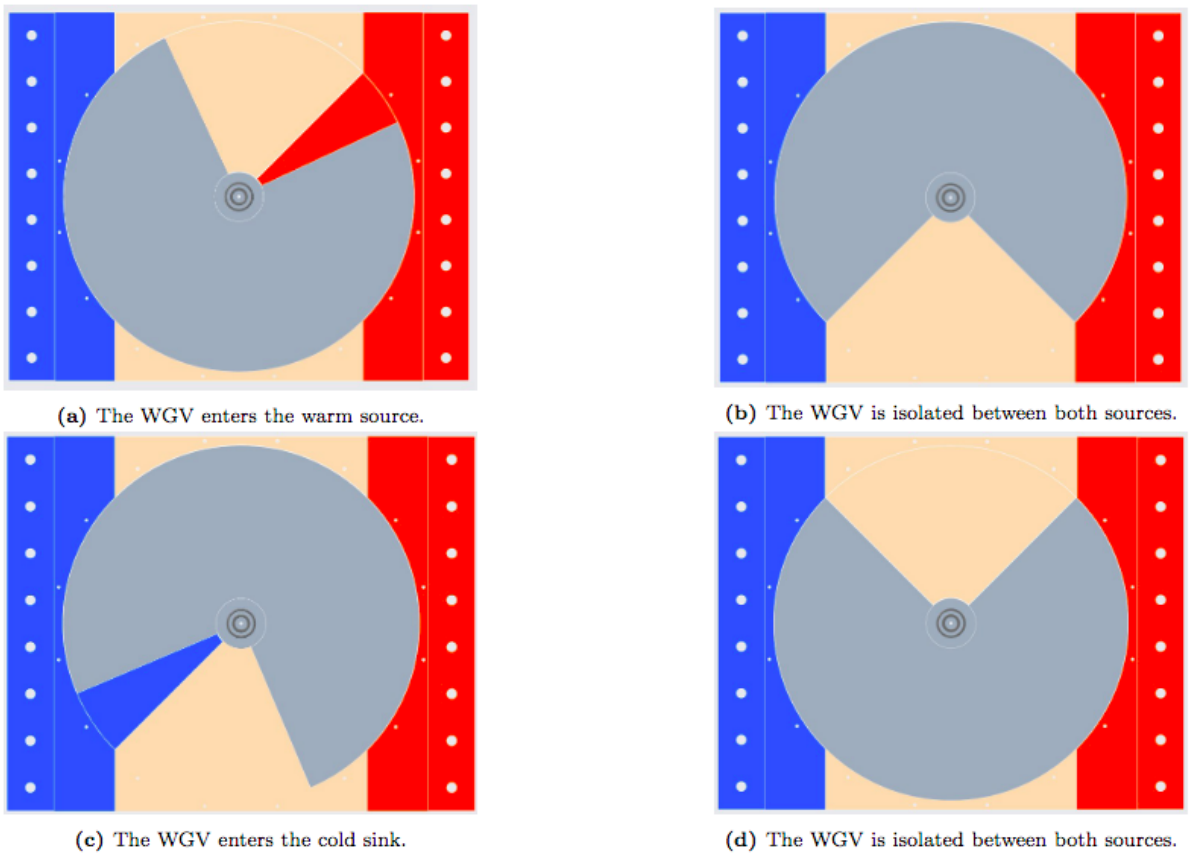

(a) The WGV enters the warm source.

(b) The WGV is isolated between both sources.

(c) The WGV enters the cold sink.

(d) The WGV is isolated between both sources.

Figure 2: An illustration of one clockwise revolution of the grey RS, and how the WGV is rotated. The blue area represents the CB and CF and the red area represents the HB and CF. [4].

The volume of air in the GREC model that is not contained within the RS, is called "dead volume". This includes, for instance, airspace between the RS and the surrounding walls or the CF, and the airspace between the shaft of the RS and the CF [4]. See Fig. 3 for the location of the dead volume in the GREC model. Some dead volume is unavoidable as the friction between the different parts of the GREC would otherwise lead to an impossible rotation, however the dead volume should be reduced in order to increase efficiency.

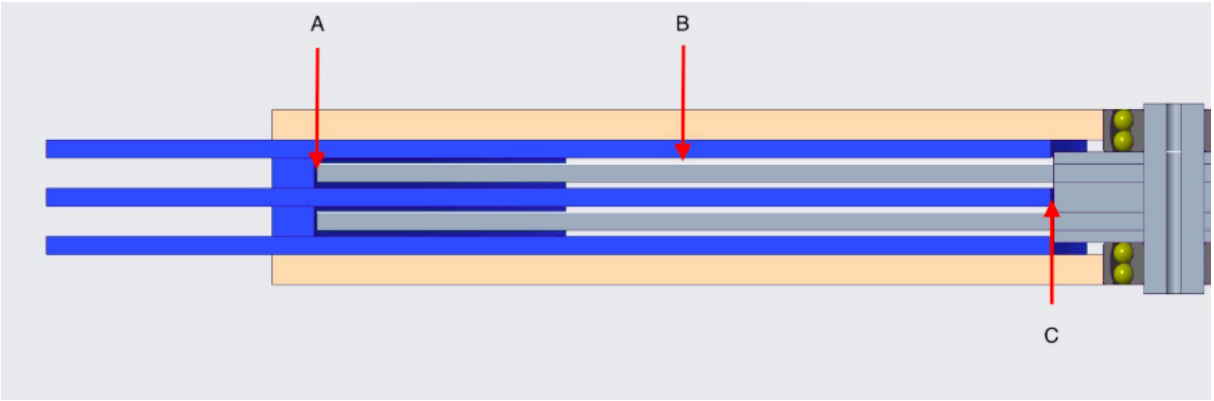

Figure 3: Illustration of the dead volume in the GREC model. 'A' is the airspace between RS and surrounding walls, 'B' is the dead volume between the RS and the conductive fins and 'C' is between the shaft of the RS and the CF [4].

This type of external heat engine has never been built before. Therefore, it is difficult to compare GREC with any existing technologies. Theoretically it can be compared to a Stirling engine [3]. Currently the GREC is still in an early development phase. To assess the maturity level of a particular technology a measurement system, Technology Readiness Levels, TRL, is used [5]. The GREC is on level 3-4 of a total scale of 9. At level 3-4, when a concept is in order to proceed into further validation in relevant environments, an experimental and analytical proof of concept must be carried out. The work is still in the laboratory environment.

nilsinside AB believes that the GREC can be used in many different applications in several scales. The reason comes from the design of the GREC which allows for a similar ratio between heat transfer area and WGV no matter size [3]. The ideal gas law then says that the pressure, and thus the work output, can be changed by either changing the volume or the temperature. This means that in order to get the same work output, GREC can be designed to be small in size with a high temperature gradient or a designed to be large with a low temperature gradient. For instance, in the transport sector with burning hydrogen where a high temperature is present, the engine could potentially be compact and small. However, in waste heat recovery or solar heat a lower temperature occurs, the engine can be largely built as a stationary unit with a large volume and piston area. According to the company, the delivered power will still be great in these applications [2].

Previous Work

A project from the spring of 2022 written by five students from the Department of Management and Engineering will be a basis for this study. They published their result: *Theoretical Proof Of Concept For The Green Revolution Energy Converter: Development of a mathematical model, material analysis and physical model improvements.*

The aim of their project was to present a theoretical proof for the concept of the GREC engine and develop the fundamentals of the technology. By establishing a mathematical model in MATLAB, results in terms of performance was investigated. The project group was additionally creating a CAD model in CREO and performed simulations in ANSYS Workbench. The fundamental principals of the Carnot-engine and the physical model from nilsinside AB were the base to construct the mathematical model. By way of explanation, the dimensions and measures of the physical model were inserted for all the calculations which was set as a base scenario. Two more scenarios were investigated for larger sizes, where a factor two and three was multiplied respectively, with the dimensions such as radius rotor, length, width, radius shaft and level of the base scenario. One level was referred to as containing one RS and one conductive fin, CF, above and below the RS. See Tab. 1 for the dimensions of the base scenario, which is the physical model from nilsinside AB.

Table 1: Dimensions and Parameters of the Physical GREC-model that was examined in previous work [4].

Dimensions/Parameters	Value	Unit
Length	0.6	[m]
Width	0.6	[m]
Conducting fin thickness	0.006	[m]
Revolving shutter thickness	0.006	[m]
Shell thickness	0.007	[m]
Case thickness	0.006	[m]
Radius rotor	0.29	[m]
Radius shaft	0.04	[m]
Levels	2	[-]

Thermodynamics simplifications, assumptions and equations regarding heat transfer were established to be able to create the mathematical model in MATLAB. For instance, air properties in their model were assumed at 20 °C and atmospheric pressure. The heat transfer between the CF and the WGV was assumed to be forced convection in a cylinder. For the base scenario, the hot and cold sources were assumed to constant at 100 °C respectively 10 °C. Additionally, heat and friction losses were neglected in the engine and the heat sources was assumed to be in contact with the WGV for half a turn of the duration of a RS. Further on, the project investigated different rotational speeds; 500 rpm, 1 500 rpm and 3 000 rpm, and temperatures of the heat source; 200 °C, 350 °C and 500 °C for a rotational speed of 1 500 rpm. The cooling temperature was the same for all simulations. For the mathematical model, the radius of the CF were divided into ten segments along the arc, since the velocity differs for all segments which affect if the flow is laminar or turbulent, see Fig. 4. This was performed to calculate the heat transfer coefficient, further mentioned HTC, for each segment and then a mean value of the HTC was used in the equation for forced convection.

Moreover, a material analysis was performed for future physical models. The material analysis was focusing on the stress and thermal simulations for the CFs, isolation and RS, to find the most suitable materials to benefit the efficiency of the GREC. Lastly, the project aimed to create a construction improvement on the physical model by using a scaled Six Sigma quality approach, to improve future models of the GREC engine.

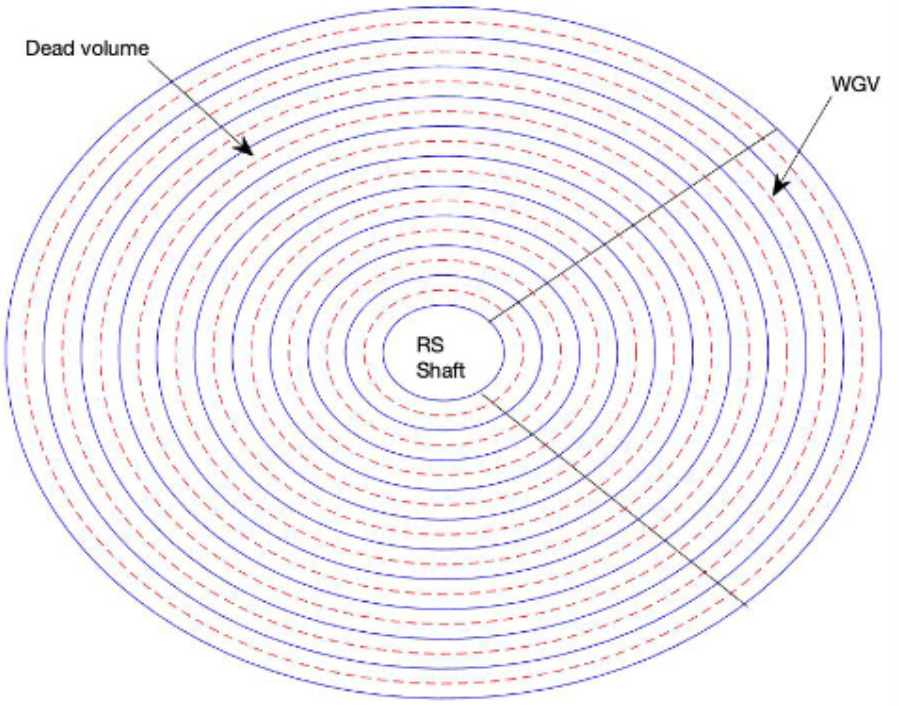

Figure 4: The ten segments are illustrated. Solid lines are the separation of each segment and the calculations for the tip speed and arc length is performed on the dash lines. The figure illustrate a whole circle but only a quarter is used for a CF [4].

The result of the previous project showed that a larger scale of a theoretical GREC model is more effective and can produce more power for all of the investigated temperatures of the heat source. A higher temperature difference between the heat source and the cold sources presented a higher power output and efficiency. This agrees with the theory of a Carnot engine, that a higher temperature difference presents a higher power output and efficiency [6]. This will be discussed more detailed later in Sec. 2.2. The rotational speeds did also have a impact on the heat transfer. A larger radius presented a higher rotational speed which in turn resulted in higher heat transfer. Furthermore, three different materials of the crucial parts were needed to present a good efficiency of the GREC model. For the CF, copper alloy was the best suited material and bakelite was the best choice for the isolation. However, copper alloy was stated as expensive and therefore aluminium was chosen as it is a cheaper option with pretty good properties. ABS (acrylonitrile butadiene styrene) with 10 % carbon fiber, a composite material, seemed to be best for the RS. It was the most light-weighted material, included in their study, which made the rotation easier and the material did also have a high yield strength and low heat transfer rate. Lastly, the scaled Six Sigma quality approach clarified that improvements of the physical model is important. However, the report did not give any concrete examples on construction improvement.

To conclude, the results from this previous report are favorable for this new project and can be used for further work on the GREC model. This new project will be a "second stage" of the previous project with further technical research of the internal parts of the GREC.

Heat Transfer Techniques

To transfer heat to and from the WGV in GREC, different heat transfer techniques can be applied. In the previous project in the spring of 2022, the temperature of the hot and cold source was set to a infinite temperature [4]. In reality, the temperature of the HB and CF are probably varying through out the parts. The temperature distribution should be affected by how the HB and CF are heated, as well as other aspects such as sizes of the CF. For heat transferring techniques in to the CF, there are several alternatives that could be suitable for the GREC. Two commonly used methods are either to fully use conductive heat transfer, or to use a combination of conductive and convective heat transfer throughout the CF. More precisely, that would mean either that the heat applied to the HB are led through the CF via only conduction, or also via convection. In the latter case, a common method is to let heat be transferred with a fluid, heat carrier, through pipes embedded in the CF. Applying this technique in the GREC model means inserting a pipe system within the CF and HB. This is called liquid heating and is used in radiators, fridges and many other heat transferring applications due to its efficiency. A drawback is that a pump system generally is needed to move the heat carrier. The required pumping power, as well as the efficiency, is affected by the properties of the heat carrier. The conductive method on the other hand, has the drawback that it is assumed to lead to slower and less even heating, but it has a very simple implementation and it is suitable for thin CFs, where pipelines cannot fit. The conductive method will further on be termed as No Pipe Heat Transfer, NPHT, and the method with a heat carrier will further on be called Pipe Heat Transfer, PHT.

Regardless, the choice of heat transferring technique, it is important to consider the rapidness and durability of different heat transferring techniques for CF and HB. The heat transfer should be fast enough to have an immediate impact of the temperature distribution on the CF, but the heat must also be enough for heating the WGV up to desired temperature. These aspects are highly affected by the radius and thickness of the CF and HB. A thicker CF and HB contain more heat energy but does also need more time to be heated up. A larger radius of the CF would also need more time for being evenly heated up which means that big temperature changes over the CF can occur. Therefore, it is reasonable to assume that a thick and big CF and HB would have more use of a PHT system than a small and thin one.

1.2 Aim

This project is part of a greater project that is divided in two with different focus areas. These two projects aim to deliver a specification of the next step of the prototype, called: Lab Model v3, which is expected to be built in spring 2023. The aim of this report is to contribute with new knowledge about the heat transfer through the HB and CF on the hot section of the GREC model. The goal is to design the HB and CF to deliver a high amount of heat to the WGV. This includes evaluating different heat transfer techniques, namely NPHT and PHT. For both the techniques, the temperature distribution within the CF and the HB, as well as the heat transfer to the WGV will be analyzed.

For NPHT the heat source will be applied to the outer surface of the HB. The NPHT analysis includes studying different radii and thicknesses of the CF and HB. Furthermore, these studies of the NPHT will be performed for two different temperatures of the heat source. The first temperature is a standard case of 100 °C, the second temperature is for a methane fuel cell application of the GREC in a vehicle where the heat source has a temperature of 500 °C [7].

For PHT, implementation of a pipeline within the CF will be examined, and different flow rates will be investigated in relation to their required approximated pumping power. The different studies of the PHT will be conducted with a heat source temperature of 100 °C of the fluid, which corresponds to the standard case of NPHT.

Research Questions

- How do different NPHT configurations, regarding radius and thickness of the CF and HB, affect temperature distribution on the CF and heat transfer to the WGV?
- How do different PHT configurations, regarding flow rate, affect temperature distribution on the CF and heat transfer to the WGV?
- How do the temperature distribution and heat transfer between the NPHT and PHT configurations differ?
- How do different heat source temperatures and possible real life applications affect which configuration is most suitable?

2 Theory

In this section, the theory and equations of heat transfer and pressure losses as well as the concept of the GREC are presented.

2.1 Equations

Eq. (1) - (5) are found in [6]. Eq. (1) is the thermal efficiency for a Carnot cycle. Eq. (2) and (3) represents relationships for an isentropic process and are valid for ideal gases with constant specific heat. Lastly Eq. (4) and (5) represents ratios where the first one is for the pressure and the second for volume which can be concluded due to T_1=T_2 and T_4=T_3 for the Carnot cycle.

$$\eta_{\text{lth}} = \left(1 - \frac{Q_L}{Q_h}\right) = \left(1 - \frac{1}{r_p^{\frac{\gamma-1}{\gamma}}}\right) = \left(1 - \frac{1}{r_v^{\gamma-1}}\right) \tag{1}$$

$$\left(\frac{T_1}{T_4}\right) = \left(\frac{P_1}{P_4}\right)^{\frac{\gamma-1}{\gamma}} \text{and} \left(\frac{T_2}{T_3}\right) = \left(\frac{P_2}{P_3}\right)^{\frac{\gamma-1}{\gamma}} \tag{2}$$

$$\left(\frac{T_1}{T_4}\right) = \left(\frac{V_4}{V_1}\right)^{\gamma-1} \text{and} \left(\frac{T_2}{T_3}\right) = \left(\frac{V_3}{V_2}\right)^{\gamma-1} \tag{3}$$

$$r_p = \left(\frac{P_1}{P_4}\right) = \left(\frac{P_2}{P_3}\right) \tag{4}$$

$$r_v = \left(\frac{V_4}{V_1}\right) = \left(\frac{V_3}{V_2}\right) \tag{5}$$

Eq. (6)-(12) are basic equations for calculations of heat transfer, found in [8]. Eq. (6) represents Fourier's heat conduction law for a wall and (7) represents Newtons law of heat transfer for convection from a surface to a fluid. Then the equation for the heat transfer coefficient is described in Eq. (8), affecting the convective heat transfer, which in turn is dependent on the Nusselt number as seen in Eq. (11) for laminar flow and Eq. (12) for turbulent flow in pipes. If Reynolds's is lower than 2300 the equation for laminar flow is used, otherwise the other equation. The value of Nusselt number is dependent on the Reynolds and Prandtl number, which are described in Eq. (9) and (10).

$$\dot{Q} = \left(Ak\frac{T_{w,i} - T_{w,y}}{b}\right) \tag{6}$$

$$\dot{Q} = \left(hA(T_w - T_{omg})\right) \tag{7}$$

$$h = \left(\frac{kNu}{L}\right) \tag{8}$$

$$Re = \left(\frac{UL}{\upsilon}\right) \tag{9}$$

$$Pr = \left(\frac{\mu c_p}{k}\right) \tag{10}$$

$$\mathrm{Nu_d} \simeq \left(\frac{0.067\mathrm{Re_d}\mathrm{Pr}\frac{\mathrm{d}}{\mathrm{L}}}{1+0.04(\mathrm{Re_d}\mathrm{Pr}\frac{\mathrm{d}}{\mathrm{L}})^{\frac{2}{3}}}\right) \tag{11}$$

Eq. (13) - (16) are basic equations coupled to fluid pressure losses and required power to pump the fluid, found in [8]. Here Eq. (13) describes component-dependent losses happening in specific parts of the pipe and Eq. (14) describes friction losses in pipes, where Eq. (15) represents the frictions loss factor in the pipes, dependent on Reynolds. Lastly Eq. (16) describes the power required to pump the fluid based on the total pressure losses and volume flow rate.

$$\mathrm{Nu_d} \simeq \left(\frac{0.038\mathrm{Re_d}^{\frac{3}{4}}\mathrm{Pr}}{1+1.5\mathrm{Re_d}^{\frac{-1}{8}}\mathrm{Pr}^{\frac{-1}{6}}(\mathrm{Pr}-1)}\right) \tag{12}$$

$$\Delta \mathrm{p_{component}} = \zeta\frac{1}{2}\rho\mathrm{U}^2 \tag{13}$$

$$\Delta \mathrm{p_{friction}} = \lambda\frac{\mathrm{L}}{\mathrm{d}}\rho\mathrm{U}^2 \tag{14}$$

$$\lambda = \frac{1}{\left(1.8\log\left[\frac{6.9}{\mathrm{Re_d}}+\frac{\mathrm{k_s}}{7.42\mathrm{r}}^{1.11}\right]\right)^2} \tag{15}$$

$$\mathrm{P_{pump}} = \Delta \mathrm{p_{tot}}\dot{\mathrm{v}} \tag{16}$$

2.2 Concept of the GREC

The GREC technology is similar to the concept of a revolving Carnot heat engine with the difference that a Carnot cycle is considered to be a reversible process [2]. The efficiency for the GREC will in reality be smaller than for a Carnot cycle due to losses in other words, not a reversible processes. As described in Sec. 2.2 the air in the GREC is moved by an electric motor from a hot CF to a cold CF, resulting in a pressure and volume change. This process can be described with Fig. 5 if compared to a Carnot cycle, where the process 1-2 and 3-4 represents a isothermal expansion and compression, respectively, achieved by the heat transferred to and from the WGV in the GREC. In the process 2-3 and 4-1, see Fig. 5, isentropic (adiabatic and reversible) expansion and compression, respectively, occur due to a completely insulated processes.

The thermal efficiency for a Carnot cycle can be calculated according to Eq. (1). $\mathrm{Q_h}$ and $\mathrm{Q_l}$ are presented in Fig. 5. The equation can be derived from Eq. (2) and Eq. (4) since the thermal efficiency is affected by temperature and pressure ratios. It can be seen that the temperature difference between positions 1-4 and 2-3 are related to the pressure difference between the same positions for an isentropic processes. It can therefore be concluded that a high temperature difference is desired to reach a high pressure difference and a high thermal efficiency. The thermal efficiency can also be derived from a volume ratio by using Eq. (3) and (5). Therefore, it can be concluded for a Carnot cycle that temperature changes between the positions 1-4 and 2-3 see Fig. 5 can be connected to volume changes. This specific equation is valid for when the working fluid is assumed to be an ideal gas and have a constant specific temperature [6]. Like for

the pressure, a higher temperature difference results in a higher volume difference which presents a higher thermal efficiency.

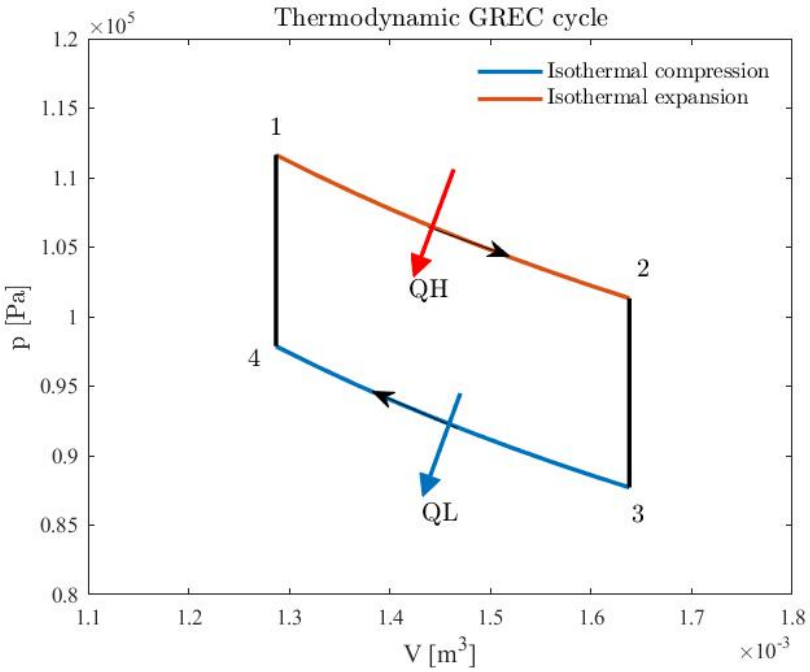

Figure 5: A representation for how a p-V diagram could look like for the GREC heat engine [4].

2.3 Heat Transfer

To enable the increase and decrease of temperature in the WGV, both conductive and convective heat transfer were taken into consideration. Heat transfer through conduction, in other words, heat transfer in solid materials, is performed within the connected block and CF. The rate of heat transfer is dependent on the thermal conductivity, the temperature and the thickness of the materials, see Eq. (6). The thermal conductivity is dependent on the type of material and temperature, and can be taken from predefined tables [8].

When considering convection, in other words, heat transfer between a solid material and a fluid, happening between the CF and the WGV, Eq. (7) is applicable. HTC is dependent on the qualities of the fluid and the flow conditions [8]. HTC can be determined with different methods, but one common way is to use Eq. (8), dependent on both the characteristic length and the Nusselt number which both are affected by the geometry and the fluid dynamics of the flow [8]. The expression of Nusselt, and the characteristic length, is often decided empirically for different fluid dynamical cases and different geometries. This means that very specific fluid dynamic cases, might not have a suitable Nusselt number equation adapted for that specific situation.

For a flow in a pipe the Nusselt number can be calculated according to Eq. (11) and Eq. (12) for laminar and turbulent flow respectively. Where the Nusselt numbers are dependent on the Reynold and Prandtl number see Eq. (9) and Eq. (10), which also are dependent on several parameters.

The heat transfer between the CF and the WGV is a forced convection that is strongly affected by the radius of CF. Different radii give different rotational speeds which impact the airflow. Generally, a higher rotational speed leads to a more turbulent airflow and a lower rotational speed leads to a more laminar flow. A turbulent flow results in a greater heat rate and if the flow is laminar the heat rate will be smaller. Since the rotational speeds is higher furthest

away from the shaft, due to a larger radius, it will result in a greater HTC compared to the area closest to the shaft [8].

2.4 Pressure losses in pipes

Pressure losses for a fluid in a pipe is caused by internal viscosity of the fluid and friction to the walls of the pipes, and obstacles in the way. It can be split into two categories: friction losses and component-dependent losses, where the latter is occurring over pipe elbows, pipe turns, valves etc. [9].There are different empirical equations that can be used to estimate these losses. The friction losses are described by different equations depending on whether the flow is laminar or turbulent, and depending on the roughness of the walls. The component-dependent losses can be calculated using empirically decided constants that differ for different types of components [8]. All pressure losses are highly dependent on the flow rate, where a high flow rate leads to a very high pressure loss.

3 Method

In this chapter, the method is described. This includes assumptions and limitations made, choices of study cases, process of creating the model in ANSYS Workbench and calculations in MATLAB. Also the simulation method applied in ANSYS Workbench and COMSOL Multiphysics together with supplementary methods as calculations, extrapolations and predictions are presented.

3.1 Assumptions and Limitations

A number of assumptions were made to be able to perform the modeling, calculations, and simulations, described in the following sections. The main assumptions and limitations are listed below:

- The HB with its connected CF in the GREC was studied and the CB with its connected CF was neglected, due to lack of available time in the project.
- Heat transfer through one single layer of the HB connected to one CF was examined to reduce the computational power and working time, compared to analyzing several identical layers of the GREC, but still obtain results applicable to a whole model.
- The temperature of the WGV entering the hot conductive fin was taken from a simulated temperature from the other project group's COMSOL Multiphysics model.
- The rpm of the RS was set to 1 500 rpm, based on previous work[4].
- The holes in the CF and HB were removed from the CAD model since they are, in reality, filled with screws which are assumed to transfer heat in a similar way as the CF and HB.
- The sides of the CF and HB were set to be isolated with adiabatic conditions, as the sides have a very small area compared to the rest of the CF, and an insulating material is surrounding these parts.
- The dead volume in GREC was neglected in ANSYS DesignModeler. The dead volume is significantly smaller than the WGV and therefore the heat transfer to the dead volume was neglected.
- The simulations in ANSYS Workbench was performed with steady state conditions since a transient case study would be complex and require high computational power and time for the simulations in this project.
- The temperature of the WGV was assumed to be constant throughout each segment of the CF, as this was the case with the values given from the other project group, which assumed that the contact time was so short that the difference could be neglected.
- The heat source temperature into the HB for the NPHT cases was assumed to be 100 °C for the standard case, based on previous work.
- The heat source temperature into the HB was assumed to be 500 °C for the NPHT model with application in a methane fuel cell in a vehicle [7].
- The temperature of the fluid of the PHT was assumed to be 100 °C for the standard case, based on previous work.

- The temperature of the heat carrier in the PHT model was assumed to be constant throughout the pipeline. This was based on the steady state conditions of the simulations and that the flow rate is so fast that the temperature reduction along the pipe is negligible.

- The fluid in the PHT was assumed to be water based on the district heating application.

- The power required for pumping the heat carrier for the PHT was only studied briefly to evaluate in relation to the chosen flow rates in the pipe. A carefully considered pumping power, for example choosing a suitable pump model, was out of scope for this project.

- The pipe in the PHT model was assumed to be milled out from the CF, in other words be consisting of aluminium.

3.2 Study cases

Firstly, the different configurations on both NPHT and PHT are presented.

Performed Studies NPHT

Studies with different parameters were performed to see how the heat distribution inside the CF and HB was affected, as well as the heat transfer from CF to the WGV. The studies performed for the NPHT model included changing the thickness of the CF and HB and changing the radius length of the CF. The heat source temperature was set to two different temperatures which were used for the described studies. The first temperature was the standard temperature of 100 °C, used also in the previous project last spring. The second temperature was based on a realistic application of the GREC, this temperature was set to 500 °C based on heat generated by a fuel cell in a vehicle and investigating an eventual implementation of the GREC in the application.

Three different thicknesses of the CF and HB were examined based on the different radii for the configurations for the temperature of 100 °C. For the configurations with the temperature of 500 °C, the radius was set to the smallest tested radius and three different thicknesses was examined. For all configurations the changing of the thickness of the model was performed in ANSYS DesignModeler. The thickness in the first case was 0.6 cm from the original model, the second case was 1.2 cm and lastly the third case was 1.8 cm. The different thicknesses to be studied were chosen based on the the impression that a thinner CF might not be feasible to produce in regards to the application. It can have a higher risk for damage or deformation if a thinner CF is exposed to mechanical stress. Therefore, it was assumed to be safer to increase the thickness instead of decreasing it, as well as a thicker CF possibly can work as a heat buffer like the HB. More material increase the capacity for storage of thermal energy in the CF and HB. In the view of those advantages, only configurations with thicker CFs were examined.

Three different radius lengths of the CF were examined, for the temperature of 100 °C, based on scaling factors. Radius x1 represented the original scaling, Radius x0.5 scaled the model with a factor 0.5, and Radius x2 was the model scaled with a factor 2. Since GREC strives to be applied in both smaller and larger applications it was interesting to investigate a smaller and larger size respectively.

A change of radius length also changes the HTC and the WGV temperature in each segment which means that the values in Radius x1, x0.5 and x2 will vary. Therefore, HTC was calculated for each case with the same method. The process to derive the values of the WGV is described under Sec. 3.5.

Table 2: Overview of the different configurations, combinations of thicknesses and radius, for the HB and CF with a heat source temperature of 100 °C.

T_{in} = 100 °C	Radius x0.5	Radius x1	Radius x2
Thickness x1	Case 1	Case 2	Case 3
Thickness x2	Case 4	Case 5	Case 6
Thickness x3	Case 7	Case 8	Case 9

Table 3: Overview of the different configurations, combinations of thicknesses and radius, for the HB and CF with a heat source temperature of 500 °C.

T_{in} = 500 °C	Radius x0.5
Thickness x1	Case 1
Thickness x2	Case 2
Thickness x3	Case 3

Performed Studies PHT

In the PHT studies, a pipe system was implemented and different studies were performed to see how the heat rate to the WGV and the heat distribution inside the CF and HB were affected. The pipe system was chosen to have a meander/ serpentine pattern, which is one of the most common patterns in floor heating. This is beneficial since the hottest section of the pipe, the beginning, can be put where the heat loss are the greatest [10]. The radius of the pipeline was kept constant at 6 mm. The length of the serial pipe was obtained from the model in ANSYS DesignModeler, where it was possible to measure the pipe. The heat source temperature of the fluid was set to 100 °C, to make the PHT configurations comparable with the NHPT configurations for the standard case. The studies performed for the PHT model included changing the flow rate of the heat carrier and simulate the results from 3 different mass flows. This resulted in a total of 3 different configurations, see Tab. 4 below. No iterations were needed to obtain the final results for the PHT configurations due to the convergence error already being small for one iteration, see further explanation in Sec. 3.5.

Three different flow rates were studied with constant radius of the pipe. The flow rates were chosen based on recommended maximum velocity of water through small pipes, in order to not get problems with noise or wear and tear of the pipes. According to [11], [12] and [13], the velocity should not exceed approximately 1-3.9 m/s, though the actual circumstances will also affect meaning that these values are not always correct. As a high flow rate is needed to get a high HTC, flow rates of 1.5 m/s, 2.5 m/s and 3.5 m/s were examined. The HTC was then recalculated for the different flow rates, where this calculation method is further explained in Sec. 3.4

Due to an assumed application in a district heating system, water was assumed being the heat carrier in the pipe. Another reason why water was chosen is because of the properties of water. Water has a low viscosity and a high thermal capacity which is desirable for a heat transfer fluid [14]. Furthermore, the pressure losses of the pipe was calculated in MATLAB in order to estimate the needed pump power needed for the PHT model. The power output, 354.95 W, from the GREC was given from the other project group and was used to evaluate the pump power in relation to the power output.

Table 4: Overview of the different study cases concerning change of flow rate of the heat carrier for a model with the thickness x3, radius x2 and a temperature on the fluid of 100°C.

T_{in}=100 °C	Flow rate 1.5 m/s	Flow rate 2.5 m/s	Flow rate 3.5 m/s
Thickness x3 & Radius x2	Case 1	Case 2	Case 3

3.3 Defining the NPHT Model

The following subsections describe how the general model of the GREC engine in ANSYS Workbench was created and how the MATLAB code originally created by the previous project group was improved [4].

Creating the Model in ANSYS DesignModeler

To create the model for ANSYS Workbench the CAD-model created previously by the spring project group was used, see Fig. 6.

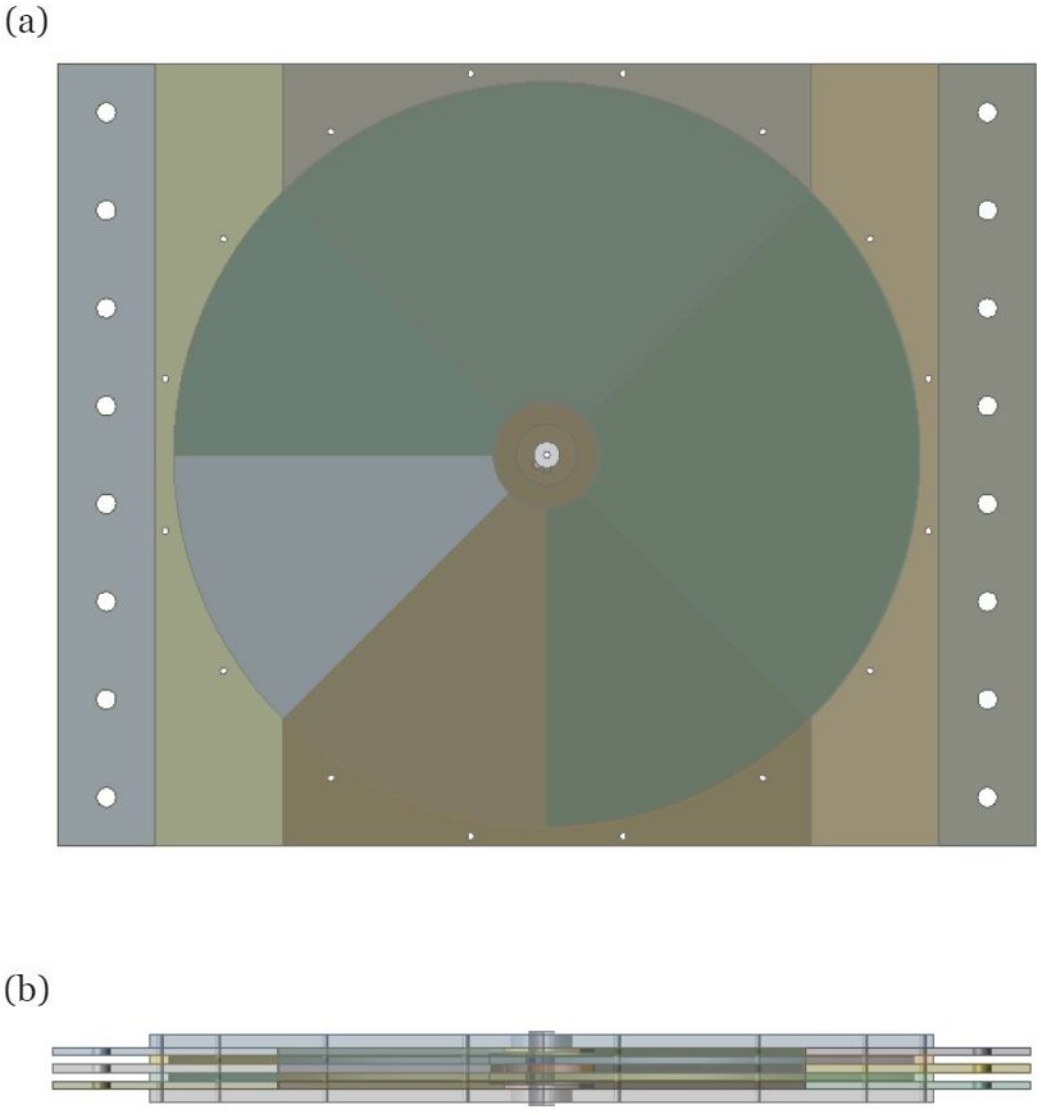

Figure 6: Two views of the CAD-models that was created in the previous work. Figure (a) illustrates the GREC from the upper point of view, (b) illustrates the GREC from a side point of view.

In DesignModeler, the geometry parts except one CF and HB was removed from the CAD-model, see Fig. 7 (a). This was done as only heat transfer through the HB and CF was studied

in this project, and also to save computational power and time. As the GREC model, in its whole, was symmetric vertically, the down scaled model could be split in half from the center line horizontally. To perform this action, a plane was placed in the center of the model's thickness and the tool slice was applied. As mentioned before, the HTC varies along the radius of the CF. Therefore the tool face split was used to create ten different surfaces, ten radial segments, on top of the geometry. This was performed to enable simulations for different HTCs for the different segments. In the model there were several holes included, see Fig. 7 (a), for screws used to enable an assemble of the model in reality. These holes in the model were filled, see Fig. 7 (b). The holes were filled using the fill function and then the faces/edges of the holes were joined with the rest of the model to make the model one whole unit with no holes using the tool boolean.

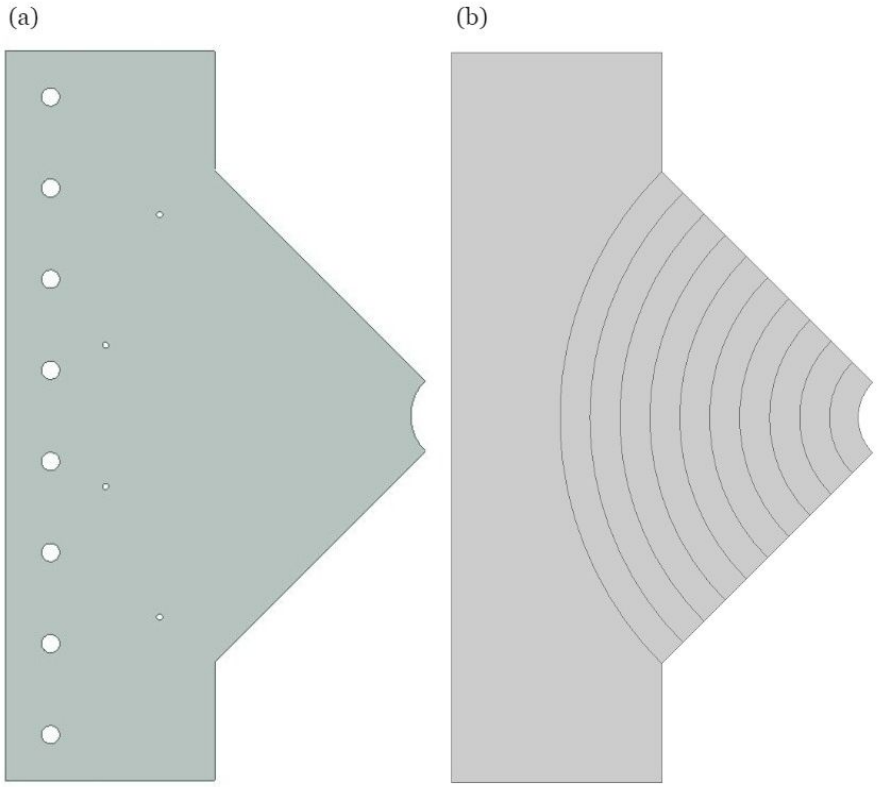

Figure 7: Figure (a) represents one CF and a HB in its original shape with holes. Figure (b) represents one CB and HB without holes and with ten different segments evenly distributed throughout the surface of the CF.

Creating the Mesh in ANSYS

Tetrahedral elements were chosen as the element type for the mesh since the tetrahedral elements can be applied for any type of geometry regardless of its shape or topology [15]. An unstructured mesh was applied on the geometry. This was due to the complexity of the geometry and the fact that there were localized positions of the model that required a higher resolution mesh [16], such as corners as well as the surfaces where heat rate appear.

Checking the mesh quality was essential to increase the accuracy for the numerical solution. The cell type, in other words, the shape of the cell, has to achieve different quality criteria to be able to gain a qualitative mesh. To measure the quality on a tetrahedral mesh the cell squish or cell skewness could either be applied, in this project, the cell skewness was evaluated [17]. The aspect ratio is also a criteria one should evaluate. These two quality measures should be evaluated before performing simulations on the domain as they have a significant impact on the accuracy of the numerical solution [17].

The skewness can be defined as the difference between the model's cell size and the optimal cell size with the equivalent volume. If the cells were highly skewed, for tetrahedral mesh a maximum skewness above 0.95 and an average value above 0.33, it can lead to convergence difficulties [17]. The aspect ratio can be defined as a measure of the stretching of a cell. When analyzing this criteria, a value close to one is preferable [18]. However, the maximum aspect ratio should be kept below 35 to get a stable solution [17].

To fulfill the criteria of the mesh quality a refinement was added. The refinement specifies the number of times the initial mesh will be refined between 1 (minimum refinement) and 3 (maximum refinement), see Fig. 8 below.

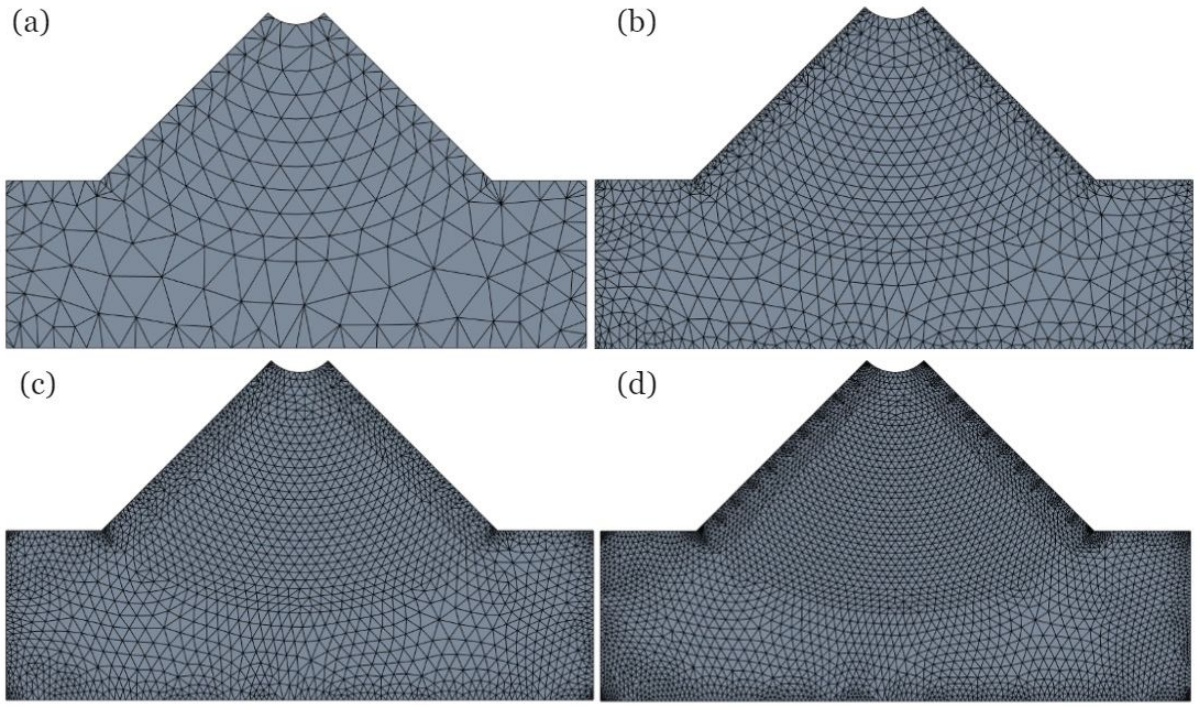

Figure 8: The four different meshes for the NPHT model. The inital mesh is shown in (a), refinement 1 in (b), refinement 2 in (c) and refinement 3 in (c).

The average and maximum values for the cell skewness and aspect ratio was evaluated for the initial mesh and each refinement, noted as Refinement 0, 1, 2 and 3 in Tab. 5. As can be seen, the the maximum and average values of the aspect ratio was relatively close to 1. As the mesh

was refined, the aspect ratio improves. The maximum aspect ratio criteria was fulfilled for Mesh 1, 2 and 3 since it was kept under 35. The maximum and average skewness got closer to the criteria as the mesh was refined, but not close enough. The criteria says that if it is not fulfilled it can lead to convergence errors, but there is no guarantee that it will not converge. Therefore the mesh was further evaluated by verifying the numerical solution to see if it converges, this is described in the following paragraph. The skewness and the aspect ratio both advocate that the most refined mesh was the most preferable.

Table 5: Maximum and average value of the skewness and aspect ratio for different refinements for the NPHT model.

Refinement	Number of nodes	Skewness		Aspect ratio	
		Max	Average	Max	Average
0	3 136	0.99969	0.92507	61.085	10.5880
1	14 599	0.99881	0.77994	19.409	5.0272
2	30 243	0.99898	0.66417	17.805	3.8745
3	57 170	0.99487	0.55863	17.590	3.3117

The first step to verify the numerical solution is to, for steady state simulations, make sure that the solution satisfies three certain criteria, RMSE (root mean square error) values, monitor points and imbalances to ensure the solution converge to steady values. The residual RMSE values need to be reduced to an acceptable value (10^{-4}), the monitor points for the values of interest need to reach a steady solution and the last criteria was that the domain needs to have imbalances of less than one percentage [19].

The monitoring point was set to be the total heat rate which is the main output of the simulations. A simulation was performed with the initial mesh and convergence was ensured for the RMSE to be less than 10^{-4}, the monitoring point was evaluated to see if it converged to a steady value and the imbalances was evaluated so it was below one percent. The number of iterations for the solution process was increased in order to allow the criteria to be fulfilled. The process was repeated for each refinement of the mesh. All of the three criteria were fulfilled for all of the different meshes. In Fig. 9 below, the result of the numerical solution is shown for the most refined mesh.

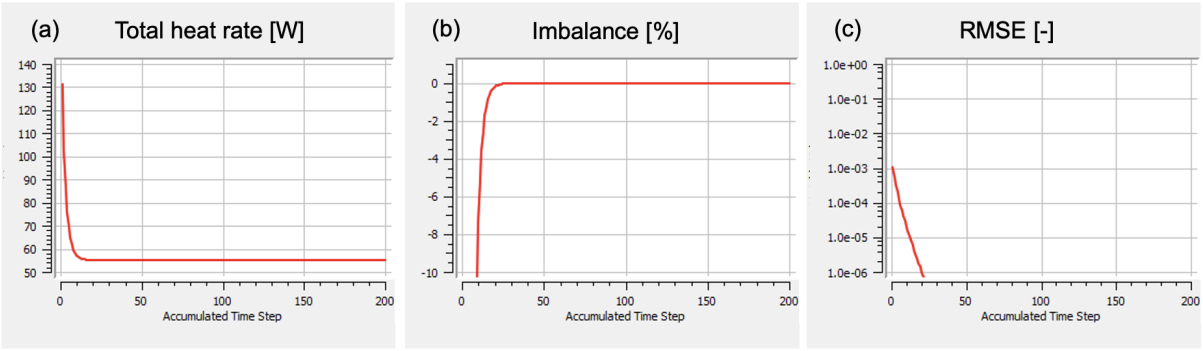

Figure 9: The numerical solution of the NPHT model with the most refined mesh consisting of the total heat rate in (a), imbalance in (b) and RMSE in (c).

The second step was a mesh independence study which was performed when the above mentioned criteria were fulfilled. The mesh independence study investigates if the simulation results are independent of the mesh or not. The result of the total heat rate for the different mesh refinements were compared with each other to display the absolute percentage difference

between finer meshes. If the total heat rate is more or less constant as the mesh is refined, the simulation result is mesh independent. In this project, the tolerance level was set to 1 %. As can be seen in Tab. 6, the change in the result when refining the mesh with a factor of 1 was above 1 %, therefore the mesh is not yet mesh independent. When refining the mesh further to 2 and 3, the change was small and therefore the mesh was considered to be accurate enough to capture the result.

Table 6: Total heat rate and the relative change compared to a simpler mesh presented for different refinements of the mesh. 0-1 is the change in result between the initial mesh and refinement 1. 1-2 is the change in result between refinement 1 and 2. 2-3 is the change in result between refinement 2 and 3.

Mesh refinement	Absolute change [%]	Mesh independent
0-1	1.65598	No
1-2	0.03621	Yes
2-3	0.19909	Yes

The analysis of the mesh concluded that, for the numerical solution and the mesh independence study, a simpler mesh (refinement 2) could have been chosen and still result in converging results. Although, due to the quality analysis of the mesh, the finest mesh was used in order to get closer to the quality criteria. The computational time is not significantly longer for the finer mesh, so this also strengthened the usage of the most fine mesh.

Setup in ANSYS CFX-Pre

In Setup in ANSYS CFX-Pre the material for the domain, in other words the CF and HB, was set to aluminium. This was based on the material analysis made by the spring project group's work [4]. The domain type was set to solid and the condition to stationary. To simulate the vertical symmetry of the model the boundary condition symmetry was applied on the top and bottom surface of the HB along with the bottom surface of the CF. Wall boundary was set for all sides representing the insulation where choice of heat transfer option was set to adiabatic. For all ten segments along the CF, the wall boundary condition was applied where the heat transfer option was set as HTC. For the boundary conditions on each segment, a HTC and temperature of the WGV were set. These values were retrieved according to the description in the next subsection. See Fig. 10 for all applied boundary conditions.

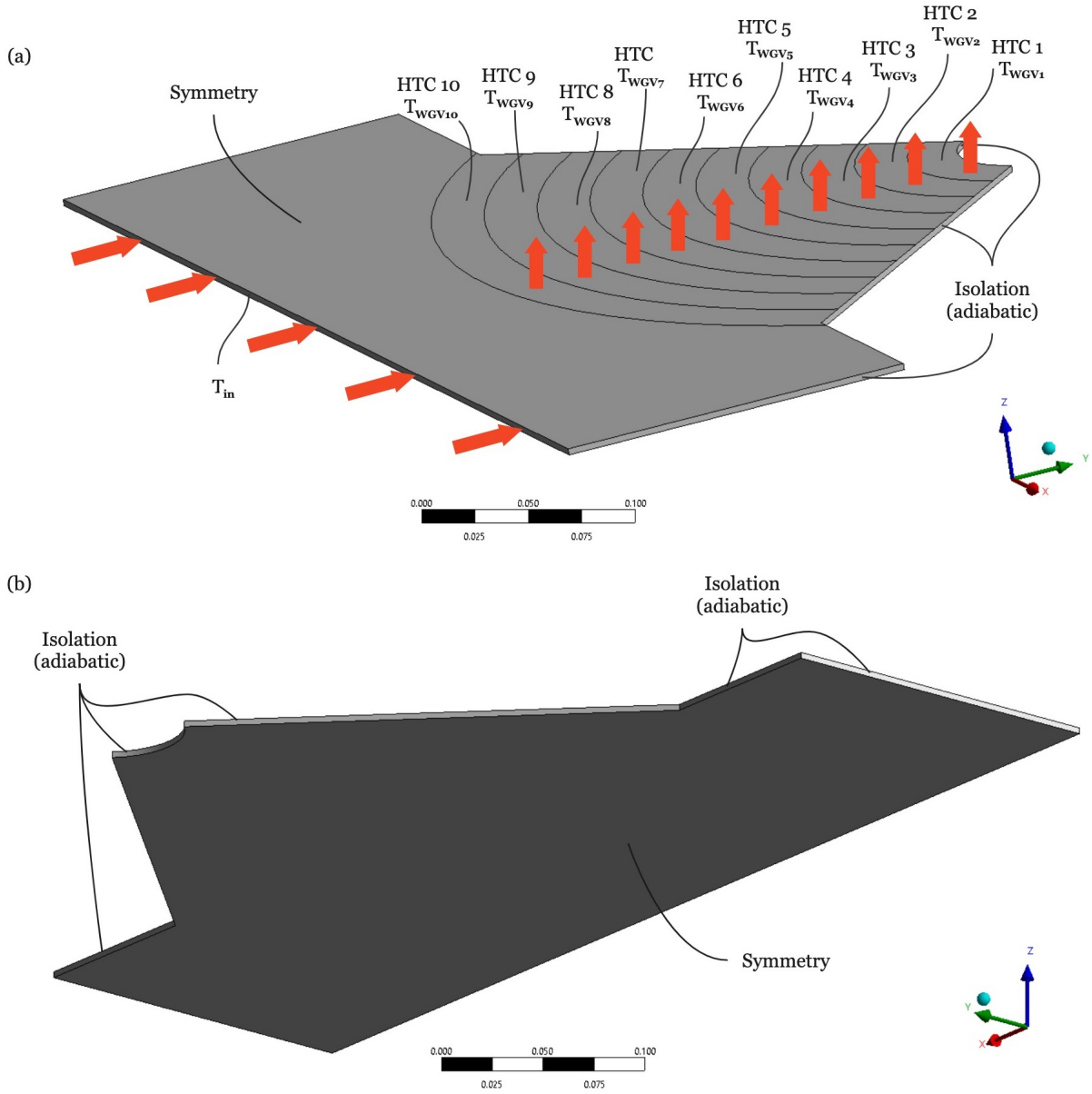

Figure 10: Figure (a) presents the boundary conditions on the WGV side of the CF and HB. The red arrows represent how the heat is transferred to the HB, and from the CF. Figure (b) presents the boundary conditions on the underside of the CF and HB. The coordinate axis is shown in both (a) and (b) to be able to more easily locate the different sides of the model.

Calculating HTC in MATLAB

The main purpose of the MATLAB model in this project was to extract HTC values for the CF, based on a reliable and accurate model in regards to dimensions, air properties etcetera. This MATLAB code was based on a MATLAB code made during the spring of 2022, by the previous project group [4]. The basis of this code was Eq. (8) - (12) which were applied for the heat transfer calculations, based on basic fluid dynamic theory. The equations are calculating forced convection in pipes, which are based on empirical expressions for the Nusselt number for a pipe geometry. This was done as the previous project group [4] chose to assume this fluid dynamical case over each of the ten segments of the fin. Forced convection is reasonable to assume as the RS is moved around and thus an external force is affecting the airflow. Regarding the geometrical

assumption, the CF as a whole does not have the geometry of a pipe, but each segment along the CF could be simplified as a pipe. The use of segments was important, since HTC is strongly related to rotational speed and therefore to radius. The code was considered well done and well suited for the purpose in this project, but it was also modified in several ways, with the aim to fit the purpose of this project. The main changes were that the scaling of the model was changed, enabling a freer scaling where each dimensional parameter could be scaled uncoupled to the other dimensions, and that the air properties were changed.

Two different MATLAB codes were created, one for a heat source temperature of 100 °C, meaning the standard case, and one for a heat source temperature of 500 °C, meaning for the application of GREC in a methane fuel cell. The calculations were divided into two codes due to that the air properties vary with the temperature and pressure. Therefore, in the standard case, the air properties were changed from being based on a temperature of 20 °C to being based on a temperature of 55 °C, which corresponded to the approximate mean temperature value in the original size of GREC. In the second code, the air properties were based on 255 °C. With other words, all air properties were changed in the codes derived from table values based on temperature and atmospheric pressure [8].

However, the density was calculated with the ideal gas law instead of using tabular values of air properties, to consider a higher pressure than atmospheric pressure. This method was applied since density affects other properties, as well as, pressure rises over the hot side of the GREC. The highest pressure in the GREC was applied to calculate the density. The highest pressure was obtained from the code from the spring's work [4]. However, the pressure calculations in the spring's project was based on a mean value of HTC over the CF. This was modified to a weighted average value based on segment areas instead. The reason for this was that HTC works over larger areas in the outer segments which therefore should have a larger impact on the mean HTC. Thus, this would increase the accuracy. The ideal gas law was also based on the mean temperature in the GREC. See Appendix. A Tab. 13 for the calculated HTC for each segment for 100 °C and Tab. 14 for the scenario with 500 °C.

3.4 Defining the PHT Model

In this following section, the method of defining the PHT model is described.

Creating the Model in ANSYS DesignModeler

As mentioned in Sec. 1.1, a NPHT configuration will probably not be able to transfer heat as efficiently for a large radius compared to a smaller radius. Therefore, the largest radius of the model in Sec. 3.3 might be in need for a different heat transferring technique, namely heat transfer through a pipeline. To be able to fit the pipe in the model, the largest thickness of the CF and HB was chosen. The model in Sec. 3.3 with the largest radius and thickness was therefore used as the base of the PHT model.

The pipeline system was created in ANSYS DesignModeler where the material inside the pipe was removed, meaning that the pipe were hollow. As previously mentioned, the CF and HB was sliced along the thickness to save computational power. The pipe were therefore modeled as semicircle as can be seen in Fig. 11 (c). Fig. 11 (a) and (b) shows the top and bottom surface of the model.

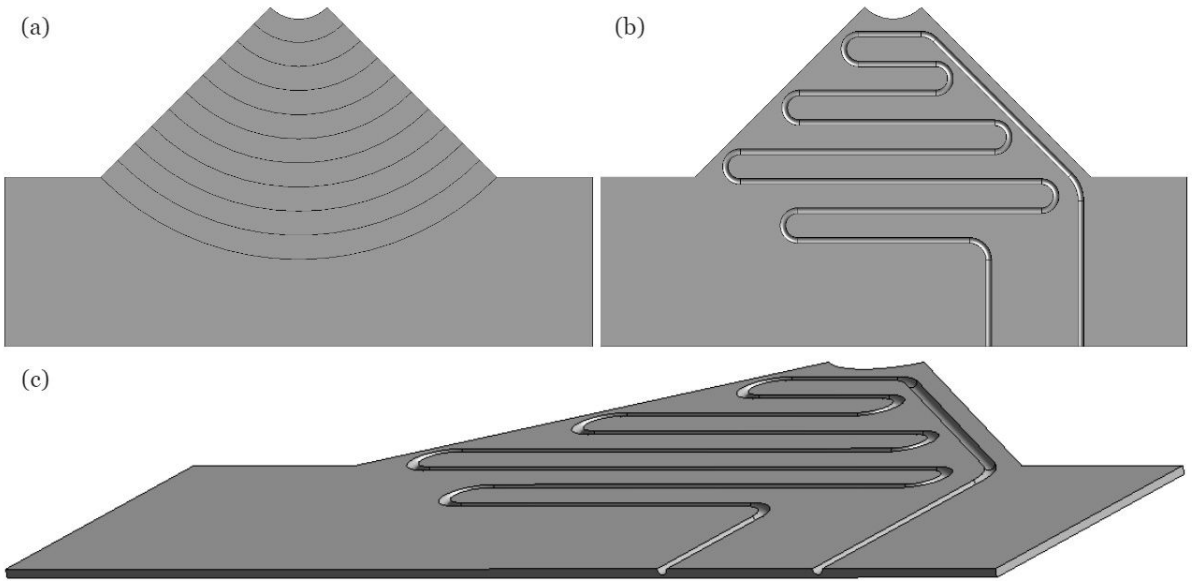

Figure 11: Illustration of the pipe system of the PHT model. The front of the model is shown in (a), the top of the model is shown in (b), and lastly an angled view of the back is shown in (c).

Creating the Mesh in ANSYS Mesh

Firstly, a tetrahedral and unstructured mesh was applied just as for the NPHT model. The quality and verification of the mesh was done in the same way as for the NPHT model, described in Sec. 3.3. To fulfill the criteria of the mesh quality a refinement was added which specifies the number of times the initial mesh was refined. The refinement was between 1 (minimum refinement) and 2 (maximum refinement), see Fig. 12 below. The time for generating the mesh with refinement 3 required a substantially longer computational time, so only refinements up to 2 were considered.

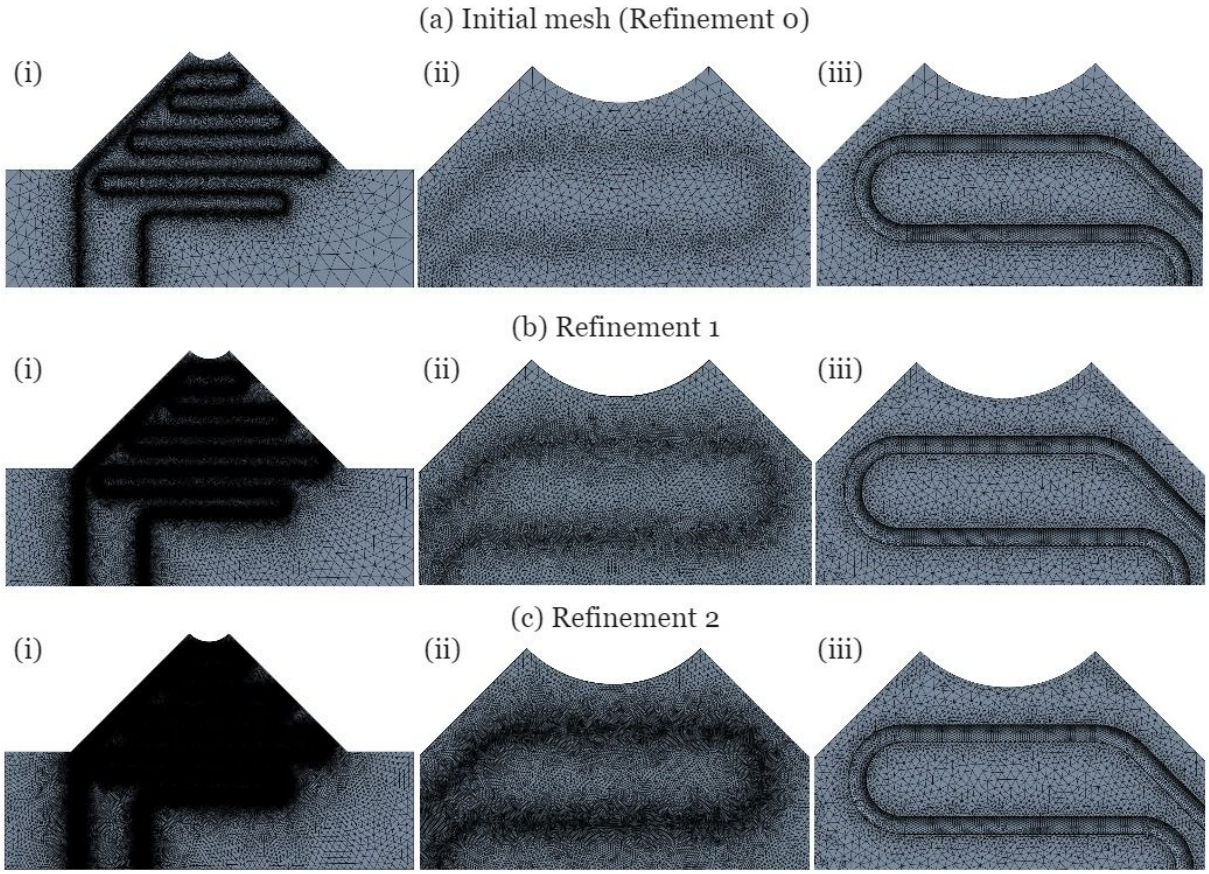

Figure 12: Illustration of the different meshes of the series PHT model. The initial mesh with no refinement is shown in (a), the mesh with refinement 1 is shown in (b) and the mesh with refinement 2 is shown in (c). All of the different meshes are shown from the front in (i), zoomed in from the front in (ii) and zoomed in from the back in (iii).

The average and maximum values for the cell skewness and aspect ratio was evaluated and presented in Tab. 7 for the initial mesh and each refinement. As can be seen, the maximum and average values of the aspect ratio gets worse as the refinement increases. However, the average and maximum aspect ratio of Refinement 0 and 1 were relatively close to the value of one compared to Refinement 2. The maximum value of Refinement 2 was drastically increased far above the value of 35, this could indicate that the solution will not be stable if this mesh refinement is used. Concerning the skewness, it can be seen that the maximum value gets worse as the mesh is refined. The average skewness is however kept below 0.33 which is preferable. One can understand that the quality criteria indicate that there may be convergence difficulties in the solution. This is further investigated in the following paragraph by studying the numerical solution of RMSE, monitor points and imbalances. Another thing to notice is that the number of nodes is drastically increased with each refinement which, together with the low quality mesh, caused the simulation time to increase.

Table 7: Maximum and average value of the skewness and aspect ratio for different refinements of the PHT model.

Refinement	Number of nodes	Skewness		Aspect ratio	
		Max	Average	Max	Average
0	155 713	0.98462	0.24740	11.379	1.8938
1	630 299	0.99521	0.27247	24.474	1.9165
2	1 391 223	1.00000	0.27264	561.48	1.9467

The same method as described in Sec. 3.3 was used for verifying the numerical solution. This was done by studying RMSE values, monitor points and imbalances. All of the three criteria were fulfilled for all of the different meshes. In Fig. 13 below, the result of the numerical solution is shown for the initial mesh with no refinement.

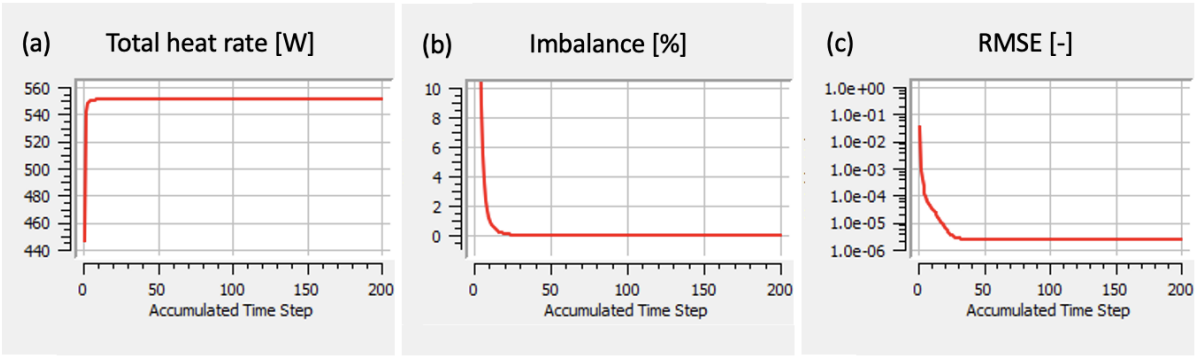

Figure 13: The numerical solution of the PHT model with the initial mesh with no refinement, consisting of the total heat rate in (a), imbalance in (b) and RMSE in (c).

A mesh independence study was performed when the above mentioned criteria were fulfilled. Just as in Sec. 3.3 the result of the total heat rate for the different mesh refinements were compared with each other to display the absolute percentage differences. The tolerance level of the absolute change was set to 1 %. As can be seen in Tab. 8, the change in the result for all the mesh refinements are below 1 %. This means that concerning mesh independence, either one of the meshes could be used.

Table 8: The relative change in heat rate compared to a simpler mesh presented for different refinements of the mesh. 0-1 is the change in result between the initial mesh and refinement 1. 1-2 is the change in result between refinement 1 and 2.

Mesh refinement	Absolute change [%]	Mesh independent
0-1	0.00272	Yes
1-2	0.00217	Yes

The analysis of the mesh concluded that the initial mesh with no refinement was preferable. This was since the skewness and aspect ratio had better values and the computational time was lower for this mesh. The initial mesh with no refinement could be chosen since the result was mesh independent and all three meshes gave converged results concerning total heat rate, imbalance and RMSE.

Setup in ANSYS CFX-Pre

The conditions in Setup in ANSYS CFX-Pre is set to the same as for the NPHT model described in 3.3 with some additional boundary conditions. The new boundary conditions, HTC and temperature of the heat carrier, are shown in Fig. 14 (b) below.

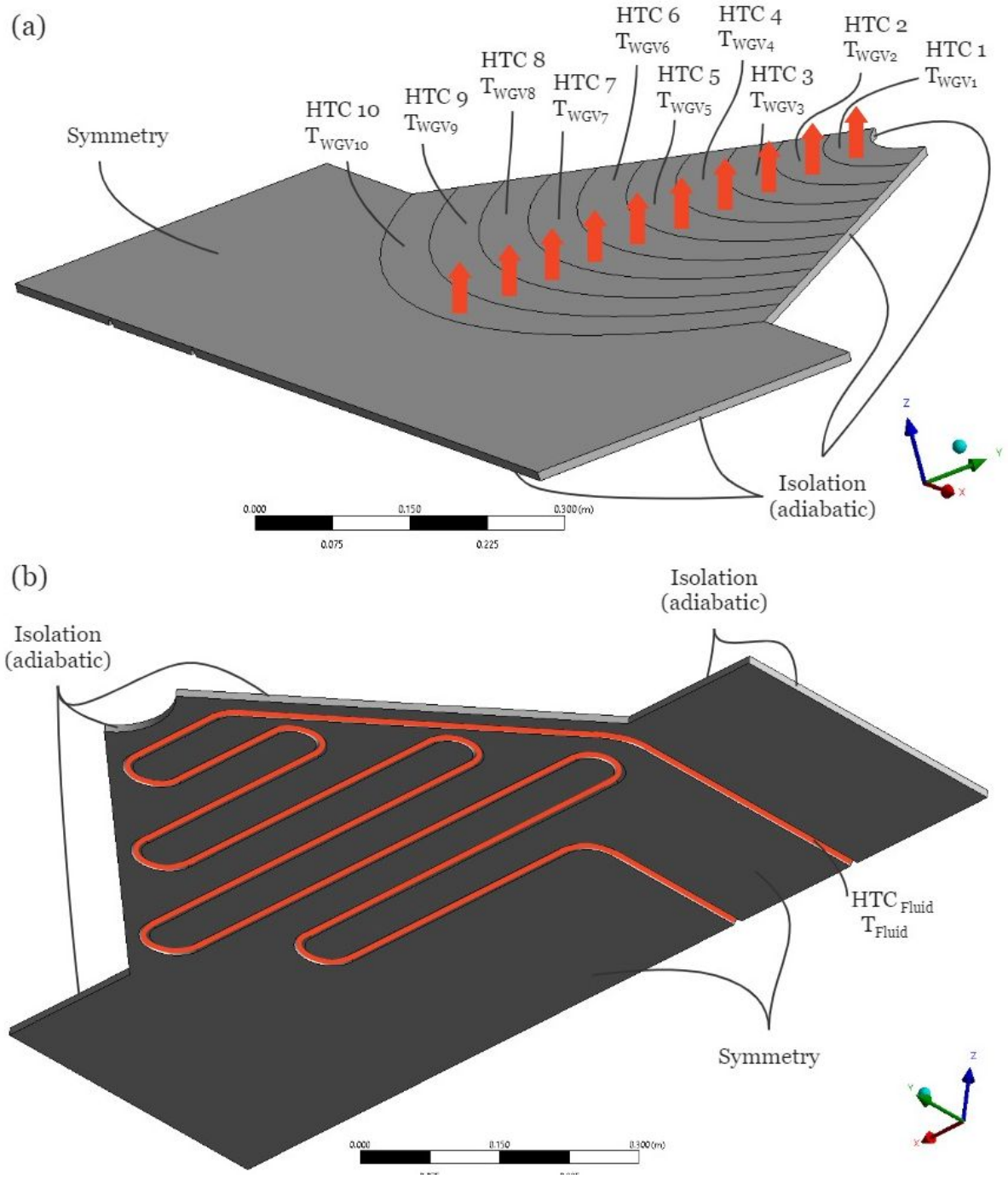

Figure 14: Figure (a) presents the boundary conditions on the WGV side of the CF and HB. The red arrows represent how the heat is transferred to the HB, and from the CF. Figure (b) presents the boundary conditions on the underside of the CF and HB. The red stripe along the pipeline system represents the heat from the heat carrier. The coordinate axis is shown in both (a) and (b) to be able to more easily locate the different sides of the model.

Calculating HTC and Pump Power in MATLAB

For the case of PHT, HTC values on the surface of the CF and on the walls of the pipe was needed, to be able to calculate the heat rate from CF to WGV. The HTC for the surface of the CF was calculated with the MATLAB code described in Sec. 3.3, where a heat source temperature of 100 °C were applied. A new Matlab code for the HTC on the walls of the pipe was created, based on the fluid properties of water and the geometrical parameters of the pipe. For the HTC of the pipe, the same equations for forced convection that was applied for the calculations for the HTC on the CF was used, see Eq. (8) - (12). The three different flow rates was inserted to present HTC for each of the flow rates.

Furthermore, MATLAB was also used to calculate the pressure losses and by this estimate the needed pumping power. First, the Reynolds number had to be calculated according to Eq. (9) and the length of the pipe had to be estimated in the ANSYS Workbench model. The pipe was assumed to be rough, and values for k_s for the aluminium walls of the pipe were found to be 0.001-0.002 mm according to [20] and [21], and 0.0015 mm according to [22], hence a value of $k_s = 0.0015$ mm was chosen. As the flow rate always resulted in turbulent flow, Eq. (14) for friction factor with turbulent flow was used, together with Eq. (13) for the component-dependent losses. The friction factor was then validated using a Moody-diagram, which is a diagram that represents Reynolds number on the x-axis and the friction factor on the y-axis, found in [8]. The value of ζ was found to be 0.2 for the 180°C turns and 0.3 for the 90°C turns, assumed that the pipe bends was smooth and flanged. The value was 0.4 for the 135°C turn, assumed not smooth and threaded bends, according to [23]. Finally, all the pressure losses were added together and with this, the needed pumping power was calculated using Eq. (16). The required input power was calculated with an assumed pump efficiency of 90%.

See Appendix. A Tab. 17 for the HTC value on the walls of the pipe and power of the pump for the different flow rates. The HTC values of the surface of the CF can be found in Appendix. A Tab. 13.

3.5 Iteration Process

To receive representative final temperature values of both the CF and WGV, iterations between the model in ANSYS and the other project group's model in COMSOL Multiphysics were performed. From the model in COMSOL Multiphysics the temperatures of the WGV for the ten different segments were retrieved for an average temperature on the CF. These ten temperatures were used in the ANSYS model to generate a new average temperature on the CF.

The iterations were performed by first applying the initial temperature of 100 °C to be the surface temperature of the CF in the COMSOL Multiphysics model. A simulation was performed and the output result was temperatures on the WGV for the ten different segments. These temperatures were applied to the ANSYS model which, in turn, gave the average temperature on the surface of CF. This CF temperature was then inserted into the COMSOL Multiphysics model which, again, resulted in new values for the temperature on the WGV. This process was initially supposed to be iterated until the temperature of the CF, for both the COMSOL Multiphysics and ANSYS model, had converged to an equal temperature. An illustrative figure of the iteration process is presented in Fig. 15.

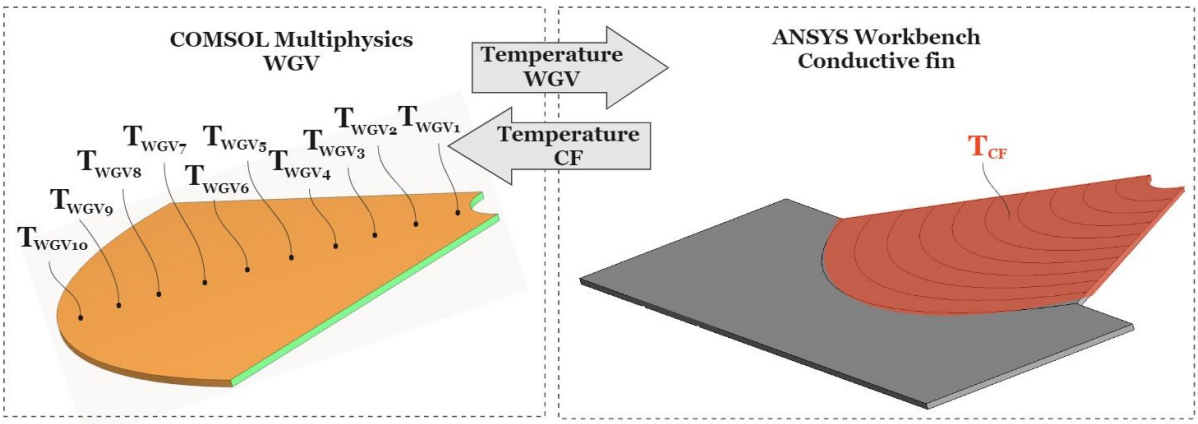

Figure 15: The figure illustrates the iteration process between the models in COMSOL Multiphysics and ANSYS.

The method described in the paragraph above would have required many iterations and much computational time. Therefore, only a number of iterations, further on called simulated iterations, were performed for one of the cases of the NPHT model. This case of the NPHT model was with the standard heat source temperature of 100 °C the dimensions x1 thickness and x1 radius. To retrieve the final temperature of the CF and WGV segments without performing further simulations, more data points from iterations were needed. These data points are further on called calculated iterations.

Three simulated iterations were made for the above mentioned case resulting in CF temperatures closer to the final value for each iteration. The percentile difference between the CF temperature applied in COMSOL Multiphysics and the simulated CF temperature from ANSYS was calculated for each iteration, see Fig. 16. This difference is further referred to as the convergence error. The percentage unit difference between the convergence errors for the iterations where calculated and was seen to be approximately 5 % between all iterations, see the table in Fig. 16 (a) and the diagram in Fig. 16 (b). This led to the assumption that this difference could be used to retrieve the calculated iterations, in other words CF temperatures.

(a)

Iteration		Temperature COMSOL Multiphysics	Temperature ANSYS Workbench	Convergence error	
[-]		[°C]	[°C]	[%]	
Simulated iterations	1	100.0	76.1	23.9	~ 5 %
	2	76.1	62.0	18.6	~ 5 %
	3	62.0	54.0	12.9	
Calcualted iterations	4	54.0	49.7	7.9	
	5	49.7	48.3	2.9	

(b)

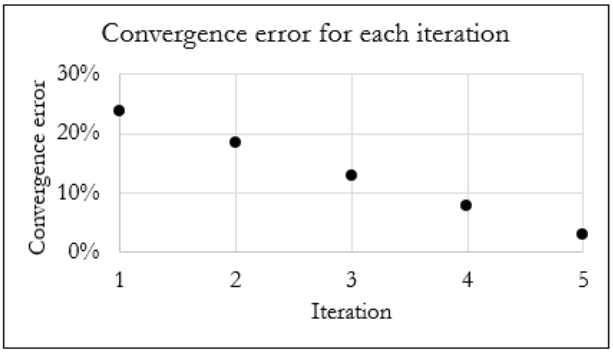

Figure 16: Figure (a) presents a table of how the temperature of the CF in both COMSOL Multiphysics and ANSYS Workbench changes for each iteration. Iteration 1-3 are simulated temperatures while iteration 4-5 are calculated. The convergence error is presented for each iteration. The difference between the convergence error for the simulated iterations are is approximately 5 %, this is applied for the calculated iterations. Figure (b) illustrates how the convergence error is decreasing for each iteration.

When all possible calculated iterations had been retrieved, the convergence errors were plotted in a diagram, see Fig. 17. An exponential trend line was then inserted based on the these data points. The trend line equation was used to extrapolate the final temperature of the CF with a convergence error of 0 %. The exponential equation was applied due to it being the equation type which represents a converging process the best.

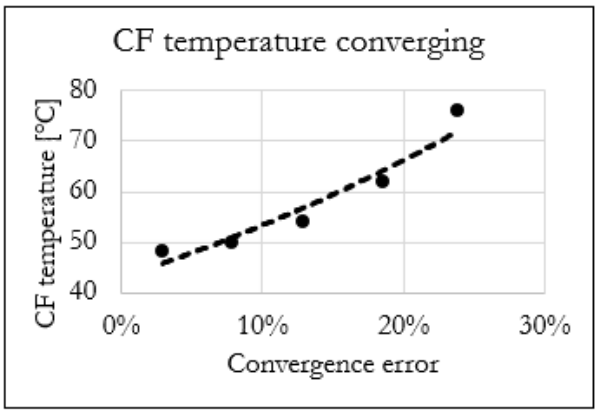

Figure 17: The diagram presents how the CF temperature changes with increasing convergence error between the COMSOL Multiphysics model and the ANSYS model. A lower temperature comes with a smaller convergence error.

For all other cases one simulated iteration had been performed, resulting in one initial conver-

gence error for each case. The percentage unit difference 5 % calculated for the earlier mentioned case, was then assumed to also be applicable on all cases. The same calculated iteration method was then used as described above, resulting in final CF temperatures for all cases.

To simulate the final total heat rate transferred from the CF to the WGV in ANSYS, the final WGV temperatures were required. There was not enough time to simulate these temperatures in COMSOL Multiphysics for all cases. Therefore, relations between the temperatures of average CF temperature and the WGV segment temperatures were used. From this relation it can be seen in Tab. 9 that for the three simulated iterations, of the standard case with x1 thickness and x1 radius, the percentage difference was approximately constant. It was thereby assumed that the final temperatures of the WGV had the same relation to the final temperature of the CF. So, to receive the final temperatures of the WGV segments the percentage difference for the first iteration was used. This was applied for all cases of the NPHT model with the heat source temperature of 100 °C.

Table 9: Percentage difference between the average CF temperature and the WGV segments for the simulated iterations of the standard case of 100 °C heat source temperature and dimensions x1 thickness and x1 radius.

Segment	1	2	3	4	5	6	7	8	9	10
Iteration 1	38.96	29.75	27.79	27.58	27.74	27.83	27.96	27.98	28.03	27.96
Iteration 2	40.06	30.31	27.48	27.23	27.27	27.27	27.32	27.29	27.34	27.22
Iteration 3	40.01	31.01	26.70	26.25	26.14	26.01	25.95	25.86	25.86	25.64

For the NPHT model with the heat source temperature of 500 °C the same method described above was used. For the PHT model, only the initial iteration was needed since the convergence error was already small enough after the first simulated iteration.

4 Results and Analysis

In this chapter, the results from the performed studies are presented starting with the standard case of 100 °C heat source temperature for the NPHT and PHT cases. Later on, the results from the fuel cell application of the NPHT model are presented. In the section the results are also analyzed, to comment the results and put them in relation to each other.

4.1 Standard Case with 100 °C Heat Source

In this section, both the results of the heat rate from the CF to the WGV and the temperature distribution are presented for the NPHT and PHT model with the standard case heat source temperature of 100 °C.

Heat Rate

The results of the heat rate for the different NPHT configurations with a heat source of 100 °C are presented in Tab. 10 below. As the radius is increased a higher total heat rate is achieved. Also, as the thickness is increased the heat rate also increases, except for the configuration with the smallest radius. This trend of increasing heat rate can be explained by the fact that a larger input area for the constant heat source on the HB enhance the energy input. In connection to this, the largest total heat rate can be seen for the model with the largest radius and thickness of the CF and HB. The heat rate equation is dependent on the CF area, so with an increased CF area, the heat rate increases as well. In addition to this, the equation also depends on the HTC values of the CF which increase as the radius increases, see Tab. 13, 14 and 15 in Appendix A.

An inconsistent result is the total heat rate for the smallest radius with different thicknesses. As can be seen in Tab. 2 the heat rate for these cases are approximately the same and are not increasing with increased thickness. This result is caused by different factors and will be further discussed in Sec. 5.2.

Table 10: Total heat rate [W] from the conductive fin to the WGV for the different studied cases.

NPHT model	Radius x0.5	Radius x1	Radius x2
Thickness x1	34.19	128.24	205.37
Thickness x2	34.57	180.56	356.94
Thickness x3	33.78	210.08	485.00

The results of the heat rate for the different PHT cases with a heat source of 100 °C are shown in Tab. 11 below. As can be seen, the heat rate is largest with a flow rate of 3.5 m/s. However, it is only slightly larger than the cases with 1.5 m/s and 2.5 m/s. By taking the pressure losses into consideration, see Appendix A Tab. 17, a lower flow rate might be an alternative since the losses are significant larger for 3.5 m/s compared to the lower flow rates. The relatively low difference in heat rate for the different cases are although strongly affected by the constant temperature assumption applied on the water.

Comparing the PHT cases in Tab. 11 with the NPHT model, with the largest thickness and radius in Tab. 10, one can see that the heat rate is significantly larger for all PHT cases. This corresponds with the heat source being closer to the WGV in the PHT model resulting in less

heat losses when distributed.

Table 11: Total heat rate [W] from the CF to the WGV for the different studied cases in the PHT model, where the temperature of the heat carrier in the pipe was 100 °C.

PHT model	Heat rate [W]
Flow rate 1.5 m/s	1 418
Flow rate 2.5 m/s	1 445
Flow rate 3.5 m/s	1 459

Temperature Distribution

In this section, the temperature distribution on the CF is presented for the different NPHT and PHT cases, with the standard case heat source of 100 °C. As can be seen in Fig. 18 for the NPHT cases the temperature is decreasing the most for the largest radius on the CF. This is an expected results due to the heat source being further away from the end point, i.e at the point of the shaft connection, for these cases compared to the others. For the different thicknesses the temperature increases when the model gets thicker for all radii configurations. This is also an expected result due to an increased area where the constant heat source is applied. The thicker fin also leads to a more even temperature distribution as it can work more as a "heat buffer". A thicker fin can contain more heat and is therefore less sensitive to high values of heat rate.

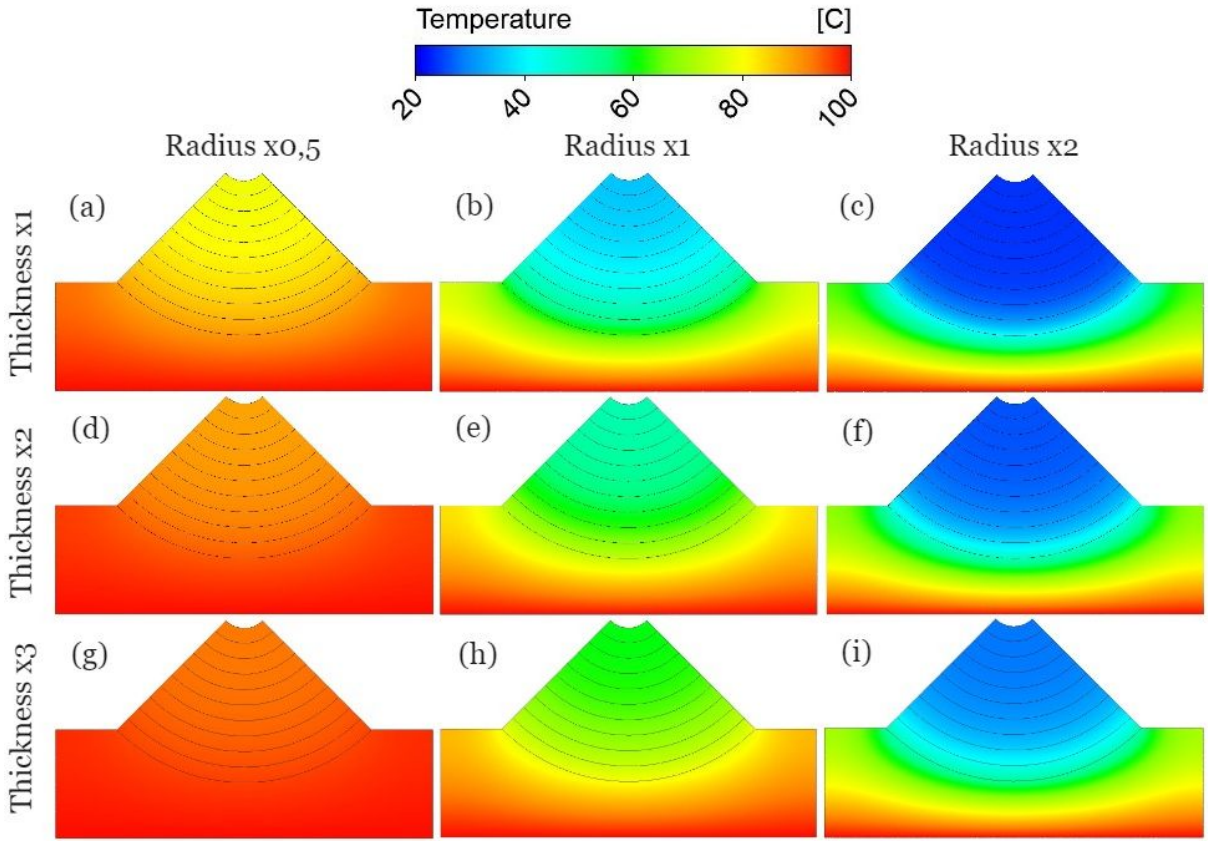

Figure 18: The figure shows the temperature distribution for the NPHT model with a heat source of 100°C. The models in the same horizontal position e.g (a), (b) and (c) presents with the same thickness and the models in the same vertical position presents the same radius. The temperature scale is presented with a scale of 20-100 °C.

In Fig. 19, the temperature distribution for the PHT configurations are presented with two different temperature scales. One scale for 20-100 °C and one for 90-100 °C.

Firstly, when comparing the NPHT model, with the largest thickness and radius in the Fig. 18, with the PHT model in Fig. 19 (a), (b) and (c), there is a large difference in the temperature distribution. For the PHT configurations the temperature difference is almost negligible when the difference for the NPHT is a lot larger. The PHT configuration can therefore be seen as favourable.

Fig. 19 (d), (e) and (f) represent a narrow temperature scale. When comparing the highest and lowest flow rates the temperature distribution is almost negligible, affected by the constant temperature assumption on the water. It is although noticeable that the temperature is a bit higher closest to the core of the RS which can compensate for a relatively low HTC coupled to the low rotational speed. This could be because the different parts of the pipe is closer to each other and therefore a higher presented temperature.

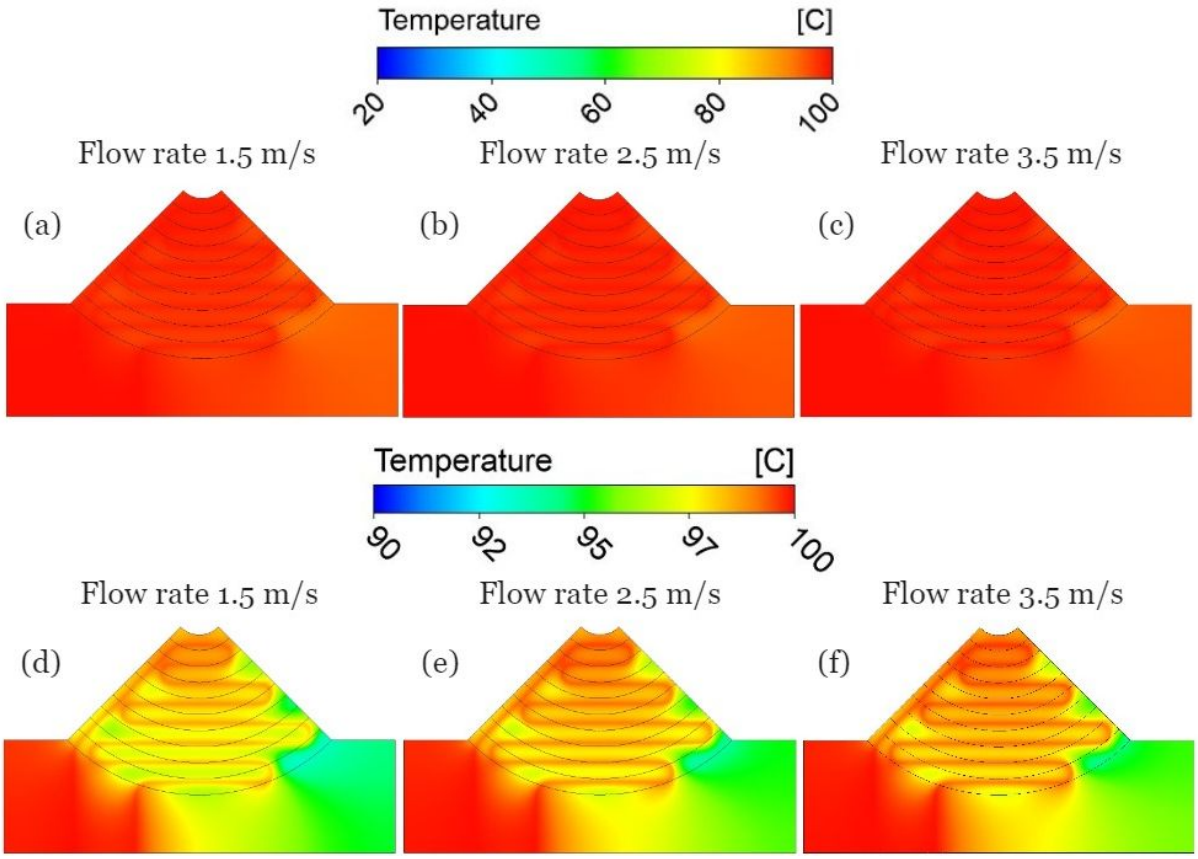

Figure 19: The figure shows the temperature distribution for the PHT model. In (a) and (d) the flow rate is 1.5 m/s, in (b) and (e) the flow rate is 2.5 m/s, in (c) and (f) the flow rate is 3.5 m/s. Figure (a), (b), and (c) are showing the model with a temperature scale of 20-100 °C. Figure (d), (e), and (f) are showin the model with a temperature scale of 90-100 °C.

4.2 Fuel Cell Application with 500 °C Heat Source

In this section, both the results of the heat rate from the CF to the WGV and the temperature distribution are presented for the NPHT model with the fuel cell application with a heat source temperature of 500 °C.

Heat Rate

The results of the heat rate for the different thicknesses of the NPHT model with a heat source of 500 °C are shown in Tab. 12 below. As can be seen, a thicker CF results in a higher total heat rate. This is since the area of the HB where the heat source is applied is increased with the thickness. This leads to a larger energy input to the HB which in turn results in the CF gaining a higher surface temperature, thus increasing the heat rate to the WGV.

Table 12: Total heat rate [W] from the CF to the WGV for the different studied cases where the temperature of the heat source was 500 °C.

NPHT model	Heat rate [W]
Thickness x1	138.070
Thickness x2	142.984
Thickness x3	144.745

Temperature Distribution

In this section, the temperature distribution is presented for the different NPHT cases with the heat source of 500 °C. As can be seen in Fig. 20, the temperature is increased as the thickness increases for each case, this is expected. As mentioned in the paragraph above, this is a result from the increased surface area of the heat source on the HB.

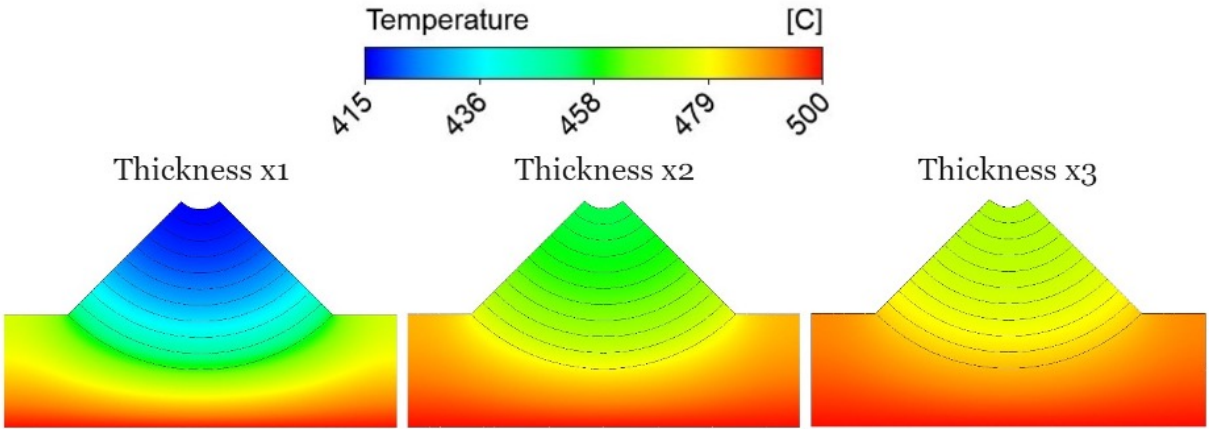

Figure 20: The figure presents the temperature distribution for the NPHT model with a heat source of 500 °C. In (a) the thickness is scaled with x1, in (b) the with x2, and in (c) with x3.

5 Discussion

This paragraph includes discussion about the project and suggestion for future studies. Assumptions and simplifications are discussed as well as their possible impacts on the result.

5.1 Defining the NPHT and PHT model

In this section, discussion about the method of defining the NPHT and PHT model is presented.

Modeling in ANSYS CFX-Pre

In ANSYS CFX-Pre a number of assumptions were applied on the model which may have an affect on the result. Firstly, the sides of the CF was set to have adiabatic conditions. Although, there is isolating material surrounding the sides of the CF, this material will not be completely isolating. There will be some heat losses through the sides of the CF which is excluded in this model. Those heat losses are considered to be small in scale compared with the result. This since the surface of the CF's sides are significantly smaller than other surfaces of the CF, and also because of the isolating material applied to the sides.

Another assumption was that the temperature of the heat carrier in the PHT model was kept constant along the pipe. Since the heat carrier transfer heat to the HB and CF, the temperature of the heat carrier would in reality decrease along the pipe. This assumption will affect the heat distribution and heat rate from the CF to the WGV. A constant temperature can be motivated by the flow rate being fast enough to impede large temperature reductions. Another reason why the temperature is invariable in this study is due to the increased complexity of the simulations. This study used steady state conditions but a transient case study would have been required to get a varying temperature along the pipe line. A transient case study would be complex and require high computational power and time. It would have been interesting to investigate further how the result from a transient case study would differ from the steady state conditions. It would also increase the accuracy of this project if the model would have been studied with transient conditions. However, the study performed in this project still gives a good picture of how the heat rate is changing with changing flow rates of the heat carrier. The study also still gives a relatively fair comparison of the PHT and NPHT results, concerning both heat rate and temperature distribution.

The temperature of the WGV of each segment was assumed to be constant in the ANSYS model. In reality it would be reasonable to think that the temperature of the WGV varies along the rotational direction of the segments, see Fig. 10, but the question is how. One could argue that the temperature should vary in many different ways. In addition to this, if the WGV has turbulent conditions one could argue that the temperature along each segment could be rather homogenous. So, the conclusion is that it is difficult to decide how the WGV temperature along each segment varies. The assumption of a constant temperature along each segment was based on the other project group that stated that the contact time between the WGV and CF is remarkably short, so that the temperature difference along each segment is negligible. Therefore, the result of the heat rate is probably not largely affected.

When building the mesh for the NPHT and PHT model, different approaches could have been applied. For example, one could have chosen a swept mesh along the pipe for the PHT model, or refined the mesh on other surfaces than the ones chosen in this project, or added different features to optimize the mesh further. In this project, the mesh is kept rather simple

with a refined automatic generated mesh. However, according to the mesh analysis, the mesh chosen for both models fulfill the most necessary criteria and it is therefore considered to be sufficient enough for the project simulations. The quality criteria, skewness and aspect ratio, for both the NPHT and PHT model do not reach the preferred limits which, as stated in Sec. 3.3, could lead to convergence issues. However, the mesh analysis included a verification of the numerical solution where the convergence of total heat rate, imbalance and RMSE is studied. All of these three parameters converged and their criteria are fulfilled. This indicated that the skewness and aspect ratio resulted in acceptable values. Furthermore, a mesh independence study was performed for the NPHT and PHT model. This study resulted in choosing a mesh refinement which gave mesh independent results of the total heat rate. So, the main outtake from the mesh analysis is that the chosen mesh is sufficient to be able to generate reliable results in the simulations.

HTC Calculations in MATLAB for the Conductive Fin

The HTC has a significant impact on the convective heat transfer which makes it important to have accurate values to achieve accurate results. The HTC values of the CF to the WGV are based on equations of forced convection in pipes. As mentioned previously in the report in 2.3, there are other ways to calculate the HTC, for instance using expressions for forced convection for a flat plane or infinite plates. However, there is today no known empirical expression for calculating the HTC for a rotating fluid along the plate with the geometry of the CF segments. Therefore, it is difficult to decide which method that is most similar to the GREC application, as well as how accurate it actually is compared to reality. To gain more insight of how the theoretical equations of HTC affects the result, one could evaluate the different relevant equations for the different geometrical cases. Another improvement would be to perform measurements on a prototype, instead of using theoretical methods. This would probably provide much more accurate HTC values, as the theories always vary from reality. However, the lack of time and a well-functioning prototype did not make it possible to perform measurements.

Further regarding the calculations, the HTC values are calculated for each segment which allows for some segments close to the shaft to have a laminar flow. In most cases, the flow is turbulent but in a few cases the flow is laminar and it is visible that in these cases, the HTC values are not following the general trends. This can be seen in appendix A for the smallest radius and the heat source temperature 500 °C. This is because different equations are applied for laminar and turbulent flow. It is natural that this partition can be a bit imprecise, but it adds some insecurities to the HTC values for the laminar flow. In reality there is no such segmentation and it is possible that the flow is actually turbulent everywhere. However, the laminar cases are few and the equations are theoretically grounded. Therefore, the accuracy of the overall results are not much affected by this.

Another aspect of the HTC values is the way the air properties were obtained when calculating the HTC. Air properties are highly dependent on two parameters, temperature and pressure. Temperature and pressure affect properties such as kinetic viscosity, density, Prandtl number, specific heat capacity and heat conductivity which all further affect the HTC. A problem with this is that the temperature and pressure naturally vary throughout the GREC. The temperature and pressure are also highly depended on the HTC, for example a higher HTC increases the heat rate, a higher heat rate leads to a higher temperature and a higher temperature of the air affects the air properties. In other words, the temperature and pressure of the air affect the HTC which affect the temperature and pressure of the air. Thus, it is a difficult to consider all this when calculating the air properties. In this project, the temperature was assumed to be constant and an average of the temperature of the hot and cold heat source temperature of the GREC when obtaining the air properties. This seem to have been more accurate for the NPHT configuration than for the PHT configuration. This is as the NPHT configuration has

less efficient heat transfer, and the final results shows that this leads to an WGV temperature that is actually rather close to the assumed one, though varying from case to case. The PHT configuration has a more effective heat transfer which leads to a WGV temperature higher than the assumed one. Therefore, it would once again have been more accurate to be more precise with the air properties in regards to their dependence on temperature, when calculating the HTC of the CF. Regarding pressure, the changed pressure of the air has not been considered for most of the air properties. In most cases, atmospheric pressure has been assumed. Only for the density, the pressure has been somewhat considered since the ideal gas law was applied for calculation of density. The density is of extra importance as it affects the other properties, for instance a high density will cause a lower value of the kinetic viscosity which results in a higher Reynolds number. These simplifications and assumptions could affect the accuracy of the HTC and should be examined further to increase the accuracy. A good use of an iterative method to obtain the air properties could be a way to do this. One way to investigate the possible errors of the HTC is to apply a sensitivity analysis of different temperatures and pressures to find out how much they affect the HTC.

However, the MATLAB code calculating the HTC shows an sufficient credibility. It is difficult to know whether the single values are accurate or reasonable, but the trends of HTC are theoretically rather reasonable. For example, a lower temperature as well as higher pressure should provide a higher density which results in a higher HTC. This is also seen in Appendix A Tab. 13 and Tab. 14, where the HTC is larger for the case with 100 °C compared to the case with 500 °C. Furthermore, the Appendix A Tab. 13 and Tab. 14, shows that the HTC is larger furthest away from the shaft which validates the code regarding the rotational speed. As mentioned previous in the report, the segments furthest away have a higher rotational speed which should generate a turbulent flow and thus higher HTC.

HTC Calculations in MATLAB for the Pipe

As mentioned above, the HTC calculations have a great impact on the heat transfer and should therefore be revised carefully. For the pipes as well as for the CF, the Nusselt equation for pipes was used to calculate HTC. This is seen as adequate for this geometrical case and should be considered correct, although empirically established and therefore a bit simplified compared to reality. The water parameters are taken for liquid water of a temperature of 100 °C although it could also be partly or fully evaporated water, in other words steam. The properties of liquid water and steam differ very much and this is therefore considered as an uncertainty in regards to the HTC of the pipe walls. Furthermore, the HTC is calculated based on a constant temperature of 100 °C which is not the actual case since heat is transferred from the water throughout the pipe. This therefore reduces the accuracy further.

Pressure Losses Calculations in MATLAB

The calculations of pressure losses in the pipe are coupled to many assumptions which in general are based on empirical studies. The component-dependent factors are not very well-motivated as it was more difficult to find really accurate descriptions of the components. For example, the component-dependent friction factor of the 135 degree turn is higher than the factor for the 180 degree turn which does not seem reasonable. However, in general, the friction losses from the roughness of the walls tend to be much larger than the component-dependent losses. This means that the assumptions regarding the component-dependent losses do not have significant impacts on the result, and would probably not affect the accuracy much. This is seen to be true also in this project, where the friction losses are about three times bigger than the component-dependent.

Another assumption made was that the effectiveness of the pump would be 90 %, which is rather high. This assumption is reasonable though since it would make sense to see if a highly

efficient pump would give results which justifies the use of a pipe system, before investigating less effective pumps. However, one should be considering when interpreting the resulting pump powers that the efficiency is highly estimated.

5.2 Iteration Process

As the COMSOL Multiphysics model of the WGV and the ANSYS model of the CF depend on each other's results for their simulations, some kind of iteration between these models was needed. The most accurate would have been to perform all of the required simulation iterations between the two models in COMSOL Multiphysics and ANSYS. The use of calculated iterations is a simplification compared to simulated iterations. The used method of a calculated iteration process consists of several assumptions that will affect the accuracy of the results.

Firstly, it was assumed that each calculated iteration leads to the same reduction in convergence error, with for example 5 percentage units for 100 °C, and also that it was the same for all different cases. To increase the accuracy of the results, one could verify if the 5 percentage unit difference is applicable for an increased number of iterations, but also if it is applicable for the different cases. It would be even more interesting to consider this in relation to the cases where the initial temperature is close to the final temperature, in other words where fewer iterations were needed. Perhaps that would result in a smaller reduction in convergence error for those cases.

Then, it was assumed that the data points, retrieved and actual, followed an exponential curve. This is precarious as extrapolation of values from an exponential curve can lead to large errors if one is not cautious, especially with few data points or close to boundaries. However, the exponential curve was found, after comparison with linear and polynomial (of 2nd degree) curves, to be the most fitting one and also the most realistic as convergence of a stable model, in general, follows an exponential expression. The curves and extrapolated values were also reviewed carefully, to see that no extrapolations error were occurring. Though, some cases had few data points. For the cases where the initial simulated iteration temperature was close to the final temperature, the data points could be as few as two. This leads to insecurities since the curve is only based on two data points. In Sec. 4 it is visible that this might have had an impact on the result for the smallest radius for with the applied standard temperature see Tab. 2, where the results are inconsistent and not expected. In reality the heat rate would probably increase for a larger thickness for the smallest radius too, as seen in the consistent trend for the larger models, but due to the applied method for the iteration of both the CF and WGV temperatures applied this trend is not seen for the smallest radius.

Further on, it was assumed that the ratio between the temperature of the CF and the segments of WGV is constant for all iterations, and thus applicable on the final extrapolated value of the temperature of the CF. In Case 2 of the standard case, it is perceived that the ratio is very similar from iteration to iteration, see Tab. 9. However, it is not certain that this is applicable to all cases and for all iterations.

Other things assumed being constant were the air properties. For each iteration the temperature change, and as mentioned earlier, the air properties and thus the HTC and resulting temperature are highly dependent on the temperature of the air. The accuracy might have been increased if the air properties were changed for each iteration where the temperature change. However, one could also argue that it is more close to reality to keep HTC at a value based on an assumed final air temperature. It is difficult to overlook the consequences of HTC in this matter and how its application to the iteration process could be improved. This is a factor of insecurity to the final results.

Finally, it was assumed that the average values of the CF temperature that are used are fully comparable to each other, which might not be the case. Meaning, the model in COMSOL

Multiphysics has a uniform CF temperature as input while the output result of the ANSYS model is temperatures for all different data points of the model, differing over the whole fin. An average temperature was thus extracted from the ANSYS model. Since one average temperature from ANSYS was used in COMSOL Multiphysics, a lot of information is lost for each iteration. This is since the differentiated temperatures are much more specific, especially since HTC vary a lot over the fin. This is seen as a rather big issue which could result in, even with properly simulated iterations, that convergence between the models might actually never be reached. This is since these kinds of errors make the models unstable.

All in all, the assumptions were many and it is difficult to overlook their consequences. They would need to be verified with more actual iterations. Furthermore, the model in COMSOL Multiphysics and the model in ANSYS comes with its own simplifications. For each simulation more error could be accumulated. Especially the COMSOL Multiphysics model, might have uncertainties not clearly considered in this project. However, the results from this iteration process are expected and follows logical reasoning, which implies a rather credible method, as seen in the analysis of the result in Sec. 4. It is also reasonable to believe that this iteration process gives more accurate results compared to the alternative of not iterating at all. Though, the results should not be used as actual numbers, but rather be analysed in order to retrieve trends and general conclusions.

5.3 Flow Rate and Pump Effect

For the PHT model, the flow rate has a large impact on the HTC. Since the flow rate is relatively high associated with a small diameter and high temperatures, the outcome in this project is a high HTC of the pipe. This is preferable for a fast heat transfer to the CF. However, for the different flow rates of the studied size of the CF, the temperature distribution of the CF and the heat rate are not varying much between the cases, see Tab. 10 and Fig. 19. The difference is more or less negligible. This means that it is possible to apply a lower flow rate to minimize the pump work. That would be preferable as with high flow rate, the pressure losses increases significantly as one can see in Appendix A Tab. 16 and Tab. 17. This would affect the overall efficiency of the GREC and must be considered in relation to the total power output from GREC.

Furthermore, in this project it is only one size of the CF that is investigated for the PHT model. It is difficult to conclude that the outcome will be the same for other sizes. Meaning that the heat rate and the temperature distribution with different flow rates might vary more or less, depending on the size of the CF.

5.4 Future Studies

When analysing the results it can be concluded that the significantly highest heat transfer from the CF to the WGV occurs when the PHT configuration is applied. With this knowledge, recommendations for future studies are focusing on, but not limited to, giving examples on different aspects to study regarding the heat transfer with a medium in pipes. The following future studies are presented in a recommended order to be conducted. The first study is recommended to be evaluated first.

Application in a District Heat System

A district heating system generally has a fluid temperature of around 80 °C [24]. When applying the method described in Sec. 3.4, it can be seen that the HTC for both the pipe and the CF surface have very similar values for 80 °C compared to for 100 °C (see Appendix A Tab. 16 and

16). This is expected as the parameters for air and water vary little with such small temperature difference. This indicates that the PHT model could most likely be adapted to a district heating system with the same results as presented for the PHT in this study. However, it would be interesting to fully investigate this.

Choice of Fluid

Water is used as the heat carrier in the pipe in this project. If applying the GREC to applications that operates in higher temperature, other heat carriers should be considered to improve the stability of the fluid. When using other fluids, the characteristics like thermal capacity, density and viscosity will be different. These characteristics affect the ability to transfer heat and the amount of power required to pump the fluid through the pipe. Synthetic oil or molten salt are two examples of fluids that have better characteristics, more temperature stable and easier to manage than water for higher temperatures [25]. Therefore, to achieve a well-functioned GREC, it is suggested to investigate and do research of fluids that suit best regarding the heat source temperature.

Distribution of the Fluid in the Conductive Fin

In this project, a configuration with one pipe and a meander/serpentine pattern in the CF is studied, see Fig. 11. For future studies, when a temperature difference of the fluid along the pipe is considered, it can be interesting to study different patterns of single pipe in the CF. Another common patterns in floor heating is bifiliar/snail pattern or double meander pattern [10]. A suggestion is to compare the different patterns to conclude which implementation that provides the greatest heat transfer and investigate how the heat is distributed throughout the CF.

Except from taking inspiration from floor heating, the design of plate heat exchangers can be investigated as well. Fluid flows in plate heat exchangers are directed through baffles where metal plates with large surface area separates the fluids. By spreading out the fluids over the plate can achieve a faster heat transfer [26]. Since plate heat transfer is a well-developed application it could be interesting to find inspirations from it and study potential implementation in the GREC.

Another future study regarding the pipe could be to investigate if more pipes rather than one will provide better heat transfer. Since the pipe in this project has a lot of bends, the pressure losses can be reduced by a design of the pipe with less bends. By applying more serial pipes with less complex design the heat transfer might be improved. Also, the heat losses through the pipes might be smaller since the length of the pipe can be reduced with more pipes. As seen in Fig. 19, there are sections of the HB and CF, that are having a lower temperature. By applying more serial pipes it could be easier to cover a larger section of the HB and CF with heat, which is preferable in a heat transfer perspective.

Change of the Fluids Phase

One way to further affect the heat transfer is to incorporate a phase change of the medium in the pipe. Today, this type of heat transfer is applied in a variety of applications like cooling systems in nuclear reactors, computers and also in applications like solar collectors and energy storage [27]. These types of pipes with a phase change is often referred to as heat pipes. Heat pipes with a phase change needs to have an evaporating and a condensation part. If the vapour is condensed in the CF the medium will extract heat to the CF working as a heat source and vice versa.

For one design of heat pipes the cross section of the pipes consists of a wicked part with a thickness connected to the inside of the pipe wall and a vapour space in the middle [27]. The

wicked part consists of a material where capillary forces can drive the condensate and vapor and where the phase change occur affecting the conductivity and therefore the pace of the heat transfer. One example with water as the medium at 150 °C, showed that the conductivity of the wicked part became several hundred times larger, compared to copper resulting in a faster heat transfer [27]. To change the heat transfer potential in this configuration, both the type of medium and the material in the wicked part can be changed.

Other configurations of heat pipes can instead directly affect the HTC between the medium and the pipe. From a study regarding different methods for calculation of HTC for condensation of mediums in pipes a method performed by Cavallini presented the best predictions closest to experimental data for condensation in horizontal smooth pipes [28]. The method from Cavallini [29] consider diameters of the pipes from 2 to 49 mm which is a range applicable on the configurations of the GREC considered in this project. A variety of different fluids were also considered in the method which could be of interest to further study for the GREC [29].

The implementation of a phase change can potentially result in a more effecitive heat transfer. To know which heat pipe configuration is the most suitable for GREC, a broader study on other available heat pipe configurations than the examples above can be studied. The implementation of the technique in a real prototype is also preferred. To know how it would function in reality.

6 Conclusions

As mentioned several times in Sec. 5, the chosen method for this study comes with several uncertainties. The conclusions drawn for the Green Revolution Energy Converter, GREC, must be read within the light of these uncertainties. However the trends seen in the results can still be considered credible, as argued for above, but exact numbers and other too detailed conclusions should be avoided.

This being said, the conclusion can be drawn that a large model, both in terms of radius and thickness, results in a higher total heat rate for the None Pipe Heat Transfer, NPHT, model. The larger the radius, the more uneven temperature distribution. However, the larger the thickness, the more even temperature distribution. The NPHT model with radius x0.5 and thickness x3 results in the most even temperature distribution for all investigated NPHT cases. The NPHT model with radius x2 and thickness x3 results in the highest heat rate. This is due to the combination of large Conductive Fin, CF, and heat source area.

A conclusion for the Pipe Heat Transfer, PHT, model is that a higher flow rate on the water does not affect the heat rate or temperature distribution on the CF much when a constant fluid temperature is applied. Therefore, based on the results from this study, a lower flow rate can be a favorable choice to save pump power.

The PHT model, as expected, present a more even temperature distribution on the surface of the CF than the NPHT model. The largest achieved heat rate from all configurations are derived from the PHT model which is almost three times larger than the heat rate derived from the NPHT model with the same dimensions. This since the temperature distribution on the CF for the PHT model is more even.

Concerning the PHT model it can be concluded that the investigated configuration with a heat source of 100 °C results in an even temperature distribution and thereby a high heat rate. The temperature in a district heating system is around 80 °C and it could be seen from this study that the Heat Transfer Coefficient, HTC, values from the CF to the Work Generating Volume, WGV, do not differ much between 80 °C and 100 °C. Based on this, it can also be concluded that this type of model design could be applicable in a district heating system.

The conclusion regarding the NPHT model is that it could also be applicable in a real life application. In this case, results imply that size of CF plays a larger role than the temperature of the heat source, in terms of the possible heat rate output. This does affect the possibility for application of the GREC within a fuel cell vehicle. If a higher heat rate is desired, a larger scale of the CF is required.

The final conclusion is that size, type of heat source and design of the GREC plays a vital role in terms of temperature distribution on CF and heat rate to WGV. The GREC have potential to be applicable in real life applications in regards of heat transfer solutions.

References

[1] Iea. Global energy Review: CO2 Emissions in 2021; 2022. [Last accessed on 12 Okt 2022]. https://www.iea.org/reports/global-energy-review-co2-emissions-in-2021-2.

[2] nilsinside AB. What is the Green Revolutionary news about?; 2022. [Last accessed on 15 Sep 2022]. https://www.nilsinside.com/nilsinside/Index-EN.html.

[3] nilsinside AB. The technology behind the GREC; 2022. [Last accessed on 15 Sep 2022]. https://www.nilsinside.com/nilsinside/Technology-EN.html.

[4] Eriksson M, Magnusson O, Haglund L, Malmdal J, Edholm G. Theoretical Proof Of Concept For The Green Revolution Energy Converter; 2022. [Last accessed on 15 Sep 2022]. https://www.diva-portal.org/smash/record.jsf?dswid=7001&pid=diva2%3A1650332&c=1&searchType=SIMPLE&language=en&query=Theoretical+Proof+Of+Concept+For+The+Green+Revolution+Energy+Converter&af=%5B%5D&aq=%5B%5B%5D%5D&aq2=%5B%5B%5D%5D&aqe=%5B%5D&noOfRows=50&sortOrder=author_sort_asc&sortOrder2=title_sort_asc&onlyFullText=false&sf=all.

[5] Tzinis I. Technology Readiness Level; 2021. [Last accessed on 15 Sep 2022]. https://www.nasa.gov/directorates/heo/scan/engineering/technology/technology_readiness_level.

[6] Zohuri B. Physics of Cryogenics; 2022.

[7] Brown M. Methane Fuel Cell runs at Temperatures Cooler than a Car Engine; 2018. [Last accessed on 12 Oct 2022]. https://www.engineering.com/story/methane-fuel-cell-runs-at-temperatures-cooler-than-a-car-engine.

[8] Storck K, Karlsson M, Andersson I, Renner J, Loyd D. Formelsamling i termo- och fluiddynamik; 2016.

[9] TEC Sciences. Pressure loss in pipes (Darcy friction factor); 2020. [Last accessed on 23 Nov 2022]. https://www.tec-science.com/mechanics/gases-and-liquids/pressure-loss-in-pipe-systems/.

[10] Multipipe. UFH Patterns; 2022. [Last accessed on 15 Nov 2022]. https://www.multipipe.co.uk/ufh-patterns/.

[11] Hy-tech. How Much Water Can Flow Through A Pipe (GPM/GPH)?; 2022. [Last accessed on 14 Nov 2022]. https://resources.hy-techroof.com/blog/how-much-water-can-flow-through-a-pipe.

[12] Engineering Toolbox. Water Systems - Maximum Flow Velocities; 2003. [Last accessed on 14 Nov 2022]. https://www.engineeringtoolbox.com/flow-velocity-water-pipes-d_385.html.

[13] BSI Engineering. Pipe Size - Rules of Thumb; 2020. [Last accessed on 14 Nov 2022]. https://bsiengr.com/wp-content/uploads/2020/11/Pipe-Size-Rules-of-Thumb.pdf.

[14] Salahuddin Qazi. Standalone Photovoltaic (PV) Systems for Disaster Relief and Remote Areas; 2017. [Last accessed on 1 Dec 2022]. https://www.sciencedirect.com/topics/engineering/heat-transfer-fluid.

[15] (a) WF. Meshing Your Geometry: When to Use the Various Element Types; 2013. [Last accessed on 11 Oct 2022]. https://www.comsol.com/blogs/meshing-your-geometry-various-element-types/.

[16] Onscale. Meshing in FEA: Structured vs Unstructured meshes; 2020. [Last accessed on 11 Oct 2022]. https://onscale.com/blog/meshing-in-fea-structured-vs-unstructured-meshes/.

[17] Ansys (b). 6.2.2 Mesh quality; 2009. [Last accessed on 11 Oct 2022]. https://www.afs.enea.it/project/neptunius/docs/fluent/html/ug/node167.htm.

[18] Dassault Systemes. Mesh Quality Check; 2021. [Last accessed on 12 Oct 2022]. https://help.solidworks.com/2021/English/SolidWorks/cworks/c_Mesh_Quality_Checks.htm.

[19] Leading Engineering Application Providers. TIPS & TRICKS: CONVERGENCE AND MESH INDEPENDENCE STUDY; 2012. [Last accessed on 11 Oct 2022]. https://www.computationalfluiddynamics.com.au/convergence-and-mesh-independent-study/.

[20] EnggCyclopedia. Absolute Pipe Roughness; 2011. [Last accessed on 24 Nov 2022]. https://www.enggcyclopedia.com/2011/09/absolute-roughness/.

[21] Engineering Toolbox. Roughness & Surface Coefficients; 2003. [Last accessed on 24 Nov 2022]. https://www.engineeringtoolbox.com/surface-roughness-ventilation-ducts-d_209.html.

[22] Chaurette J. PIPE ROUGHNESS VALUES; 2003. [Last accessed on 24 Nov 2022]. https://www.pumpfundamentals.com/download-free/pipe_rough_values.pdf.

[23] Cengel Y, Turner R, Cimbala J. Fundamentals of thermal-fluid sciences [5th edition]; 2016. McGraw-Hill Education.

[24] Gadd H, Werner S. Achieving low return temperatures from district heating substations; 2014. [Last accessed on 12 Oct 2022]. https://www.sciencedirect.com/science/article/pii/S0306261914009696#b0015.

[25] Process Heating Magazine. How to Choose the Right Heat Transfer Fluid; 2010. [Last accessed on 7 Dec 2022]. https://www.dow.com/content/dam/dcc/documents/en-us/tech-art/176/176-01616-01-how-to-choose-the-right-heat-transfer-fluid.pdf?iframe=true.

[26] R Wright, J Wright, C Cabet. Material Performance and Corrosion/Waste Materials; 2012. [Last accessed on 1 Dec 2022]. https://www.sciencedirect.com/science/article/pii/B9780080560335000999.

[27] Reay D, Kew P, McGlen R. Theory, Design and Applications; 2014. [Last accessed on 23 Nov 2022]. https://ebookcentral.proquest.com/lib/linkoping-ebooks/reader.action?docID=1457874&ppg=4.

[28] Ribatski G, Silva JDD. Condensation in Microchannels; 2015. [Last accessed on 23 Nov 2022]. https://ebookcentral.proquest.com/lib/linkoping-ebooks/reader.action?docID=4003912&ppg=4.

[29] Cavallini A, Col DD, Doretti L, Matkovic M, Rossetto L, Zilio C. Condensation in Horizontal Smooth Tubes: A New Heat Transfer Model for Heat Exchanger Design; 2006. [Last accessed on 23 Nov 2022]. https://eds.s.ebscohost.com/eds/pdfviewer/pdfviewer?vid=1&sid=3dd3fb62-e0f4-4e26-bad5-920fe884cdc8%40redis.

A Appendix

Table 13: The radius (r) and HTC (h) of each segment in the conductive fin for radius x0.5, x1 and x2 and an inlet temperature of 100 °C.

	Segment	r	h
		[cm]	[W/(m^{2}K)]
Radius x0.5	1	3.16	33.32
	2	4.32	43.70
	3	5.48	53.17
	4	6.64	62.06
	5	7.80	70.50
	6	8.96	78.58
	7	10.12	86.37
	8	11.28	93.91
	9	12.44	101.24
	10	13.60	108.37
Radius x1	1	6.46	52.49
	2	8.92	69.51
	3	11.38	85.11
	4	13.84	99.72
	5	16.30	113.60
	6	18.76	126.88
	7	21.22	139.68
	8	23.68	152.06
	9	26.14	164.09
	10	28.60	175.81
Radius x2	1	13.06	84.62
	2	18.12	112.73
	3	23.18	138.48
	4	28.24	162.60
	5	33.30	185.49
	6	38.36	207.40
	7	43.42	228.51
	8	48.48	248.94
	9	53.54	268.79
	10	58.60	288.12

Table 14: The radius (r) and HTC (h) of each segment on the CF for radius 0.5x with an inlet temperature of 500 °C.

	Segment	r	h
		[cm]	[W/(m^{2}K)]
Radius x0.5	1	3.16	38.56
	2	4.32	39.38
	3	5.48	39.84
	4	6.64	55.42
	5	7.80	62.87
	6	8.96	69.99
	7	10.12	76.84
	8	11.28	83.47
	9	12.44	89.91
	10	13.60	96.18

Table 15: The radius (r) and HTC (h) of each segment on the CF for radius x2 with an inlet temperature of 80 °C.

	Segment	r	h
		[cm]	[W/(m^{2}K)]
Radius x2	1	13.06	84.46
	2	18.12	112.51
	3	23.18	138.21
	4	28.24	162.27
	5	33.30	185.11
	6	38.36	206.98
	7	43.42	228.04
	8	48.48	248.43
	9	53.54	268.23
	10	58.60	287.53

Table 16: The flow rate (u) and pump power (W) of the heat carrier within the pipe, and the HTC (h) of the pipe within the conductive fin for an inlet temperature of 80 °C.

u	P	h
[m/s]	[W]	[W/(m^{2}K)]
1.5	1.86	10 956
2.5	7.95	16 364
3.5	20.81	21 303

Table 17: The flow rate (u) and pump power (W) of the heat carrier within the pipe, and HTC (h) of the pipe within the conductive fin for an inlet temperature of 100 °C.

u	P	h
[m/s]	[W]	[W/(m^{2}K)]
1.5	3.94	11 517
2.5	16.90	17 105
3.5	44.34	22 188